universität wien

MASTERARBEIT / MASTER'S THESIS

Titel der Masterarbeit / Title of the Master's thesis

Extracellular vesicles and their impact on the epithelial plasticity of hepatocellular carcinoma cells

verfasst von / submitted by

Adriana Martinez Turtos

angestrebter akademischer Grad / in partial fulfillment of requirements for the degree of

Master of Science (MSc)

Wien, 2018 / Vienna, 2018

Studienkennzahl lt. Studienblatt / Degree programme code as it appears on the student record sheet:	A 066 830
Studienrichtung lt. Studienblatt / Degree programme as it appears on the student record sheet:	Molecular Microbiology, Microbial Ecology and Immunobiology
Betreut von / Supervisor:	Ao. Univ. Prof. PhD. Wolfgang Mikulits

TO LEONOR M. TURTOS CARBONELL
&
ARTURO I. MARTINEZ PULIDO

AKNOWLEDGEMENTS

This master project is a result of the combined initiative and effort of several parts.

I thank my supervisor Prof. Wolfgang Mikulits for giving me the chance of making research in such an interesting topic, for his talented way to guide my professional formation during this year, for his patience and good mood.

I thank our research team in special, Gerhard Weber for teaching me in the best way the experiments I performed in the lab, guiding my research work, helping with the manuscript and for making happy those days.

I thank Heidemarie Huber for performing an essential part of the project, supporting my experimental work and being always present in the lab.

This thesis project was made in collaboration with the Neuro-oncology department of the General Hospital of Vienna, Austria. I thank PhD, Sibylle Madlener for all the measurements at any time, for her interest in the project, her patience, and for her useful advices.

I thank Prof. Andreas Spittler for his disinterested technical support that made possible part of our experimental work.

Thanks to my parents, sister Ro, brother-in-law, family and close friends for being always present for me.

CONTENTS

ABSTRACT

Globally, liver cancer represents the sixth most common cause of cancer and ranks second in the mortality of cancer patients. Hepatocellular carcinoma (HCC) is the most common subtype of primary liver cancer. Poor survival of HCC patients reflects the lack of specific biomarkers for early diagnostics as well as high levels of metastasis and recurrence after surgical resection. This highlights the urgent need of anti-cancer therapies to combat HCC. Tumor-derived exosomes are bio-nanoparticles involved in several steps during tumor development. For instance, these small extracellular vesicles (sEVs) derived from highly metastatic human HCC cells induce higher migration and invasion of non-motile immortalized human hepatocytes in a process that resembles epithelial to mesenchymal transition (EMT). Therefore, elucidating the role that these sEVs are playing in the metastatic cascade of HCC could bring novel insights for design of new targeted therapies. In order to investigate whether sEVs derived from EMT-transformed HCC cells have an impact on the cell plasticity of epithelial HCC cells, *in vitro* EV treatment of well-differentiated HepG2 cells was performed. EVs isolated from mesenchymal HCC cells induced changes in the epithelial plasticity of HepG2 cells by downregulation of E-cadherin transcript levels. Reduction of E-cadherin expression was independent of the transcriptional repression exerted by EMT-transcription factors and upregulation of other mesenchymal markers. Previous to EV treatment of HepG2 cells, EVs derived from cell culture conditioned medium of mesenchymal-like HCC cells were characterized by their size and the presence of a combination of markers specific for sEVs. Characterization of those EVs by nanoparticle tracking analysis demonstrated that upon isolation by differential ultracentrifugation (DUC), the sEV fraction represented more than 50% of the EV population. The use of a membrane affinity-based commercial kit for isolation of EVs yielded a lower representation of sEVs as compared to DUC. Characterization of DUC-isolated EVs by immunoblotting resulted in co-enrichment of the tetraspanin members CD63 and CD81, unique presence of TSG101 and the lack of the endoplasmatic reticulum protein GRP78. In addition, CD63-GFP-expressing HCC cells were generated with the aim of investigating the role of EVs in pre-metastatic niche formation *in vivo*. Those HCC cells released GFP-labeled EVs as demonstrated by immunodetection, immunofluorescence microscopy and flow cytometry analyses. Further selection of single cell clones was performed for future EV education of immunodeficient mouse models prior to xenotransplantation. Altogether, this study shows the role of EVs as messengers mediating cell-to-cell communication between mesenchymal-like and epithelial HCC cells leading to induction of changes in the epithelial plasticity. GFP-labeled EVs were isolated by DUC as the method of choice, characterized and selected to provide a valuable tool for studying *in vivo* formation of the pre-metastatic niche of HCC cells.

ZUSAMMENFASSUNG

Leberkrebs ist der weltweit sechsthäufigste maligne Tumor, der zur zweithäufigsten Mortalität aller Krebserkrankten führt. Das hepatozelluläre Karzinom (HCC) ist der vorherrschende primäre Leberkrebs. Die schlechte Prognose von HCC Patienten ist mit fehlenden Biomarkern für die diagnostische Früherkennung sowie einer häufig auftretenden Metastasierung nach chirurgischer Entfernung des Primärtumors begründet. Darum sind geeignete Diagnosen und Therapien für die erfolgreiche Bekämpfung des HCC von äußerster Wichtigkeit. Tumor-abgeleitete Exosomen sind kleine extrazelluläre Vesikel (sEVs), die von Tumoren produziert werden und diese in vielen ihrer Entwicklungsstadien beeinflussen und regulieren können. Kürzliche Studien haben gezeigt, dass metastasierende HCC Zellen sEVs freisetzen können, welche die Migration und Invasivität von differenzierten Hepatozyten mittels eines epithelial zu mesenchymalen Transition (EMT)-ähnlichen Prozesses induzieren. Das Verständnis der sEV Funktionen in der metastatischen Kaskade des HCC könnte die Basis für die Entwicklung einer neuen zielgerichteten Therapie sein. In dieser Studie wurden differenzierte HepG2 Zellen verwendet, um herauszufinden, ob sEVs von EMT-transformierten HCC Zellen einen Einfluss auf die Zellplastizität von epithelialen Zellen haben. Die, von mesenchymalen HCC Zellen gewonnen, EVs konnten eine Veränderung der epithelialen Zellplastizität der HepG2 Zellen durch Verminderung der E-Cadherin Expression induzieren. Die reduzierte E-Cadherin Expression war unabhängig von einer verstärkten Abundanz mesenchymaler Marker oder charakteristischen EMT-Transkriptionsfaktoren. Die für das Experiment verwendeten EVs wurden vorab bezüglich ihrer Größe und EV-spezifischer Marker charakterisiert. Zudem wurde der Anteil der sEVs innerhalb der EV Population mittels Nanopartikelanalyse bestimmt. Die durch differentielle Ultrazentrifugation (DUC) gewonnene sEV–Fraktion betrug über 50%. Kommerziell erhältliche Kits, die auf Membranaffinität basieren, zeigten eine geringere sEV Ausbeute verglichen mit der DUC-Methode. Western Blot Analysen der DUC isolierten EVs ergaben eine Anreicherung mit den Tetraspanin-Proteinen CD63 und CD81 sowie das Vorhandensein von TSG101 und das Fehlen des Endoplasmatischen-Reticulum Proteins GRP78. Zusätzlich wurden CD63-GFP exprimierende HCC Zelllinien für die Freisetzung von GFP-markierten sEVs generiert, die für weiterführende *in vivo* Untersuchungen zur Funktion einer prämetastatischen Nische eingesetzt werden sollen. CD63-GFP markierte EVs wurden mittels Immunfluoreszenzmikroskopie, Western Blot Analyse und Durchflusszytometrie nachgewiesen und einzelne Zellklone selektiert. In diesen Experimenten soll der Effekt von EVs auf die Ausbildung einer prämetastatischen Nische nach Xenotransplantation in immundefizienten Mäusen geklärt werden. Zusammenfassend zeigt diese Studie die Rolle von EVs als Vermittler in der Zell-Zell Kommunikation zwischen mesenchymalen und epithelialen HCC Zellen auf. Es konnte gezeigt werden, dass EVs von mesenchymalen Zellen

eine Änderung in der Plastizität von epithelialen Zellen induzieren. Zusätzlich wurden GFP-markierte EVs mittels der für uns am besten geeignete Methode der DUC isoliert, charakterisiert und selektiert. Diese Zellmodelle stehen nun als Werkzeug für die Untersuchung der prämetastatischen Nische des HCC zur Verfügung.

I INTRODUCTION

I.1 Development of hepatocellular carcinoma

Primary liver cancer constitutes the sixth most common cancer worldwide and ranks at the second place in cancer mortality. Cholangiocarcinoma and hepatocellular carcinoma (HCC) are the two major types of liver cancer, the latter accounting for approximately 80% of all cases[1]. Major HCC risk factors to promote malignant development of the hepatocytes include viral infections with hepatitis B or C, aflatoxin B1 exposure, alcohol abuse, obesity, diabetes and metabolic syndrome, being genetics a minor contributor. Irrespective of the etiology, the neoplastic changes usually occur in a chronic necro-inflammatory environment that in most cases progresses sequentially from fibrosis to cirrhosis which could culminate in HCC development[2]. Taken into account that HCC is typically diagnosed at late tumorigenic stages, mostly due to the lack of suitable biomarkers for early detection[3], the median survival after diagnosis is approximately between 6 and 20 months[4]. Even though there have been progress in HCC-targeting therapies, the high metastatic burden in the liver itself and distally in lungs, lymph nodes and bones impairs the survival of those patients. In this regard, the dissemination of tumor cells might account for HCC recurrence after surgical resection[5]. Therefore, there is an urgent need for novel therapeutic approaches to combat HCC.

HCC is characterized by a wide spectrum of molecular heterogeneity attributed to the etiology of underlying chronic liver diseases and the influence of the tumor microenviroment[6]. As HCC is frequently linked to chronic liver damage, the oncogenic transformation is a result of persistent inflammatory processes, cell damage and constant cellular turnover which promote repair events highly prone of errors. In addition, selective pressure on the healthy and new hepatocytes due to the changing microenvironment promotes the survival of malignant cells[3].

Liver injury is accompanied by acute inflammation which can be perpetuated and consequently reach a chronic state. The inflammatory process involves the recruitment of non-resident immune cells into the liver which orchestrate a strong inflammatory response together with the immune cells homing the liver such as Kupffer cells, dendritic cells, T lymphocytes and natural killer (NK) cells[2]. In this necro-inflammatory context in the presence of oxidative stress, non-parenchymal liver cells, mainly hepatic stellate cells (HSCs) become activated and trans-differentiate to α-smooth muscle actin (α-SMA)-expressing myofibroblasts (MFBs). These fibroblasts secrete extracellular matrix (ECM) components such as fibrillar collagen, fibronectin and tissue inhibitors of metalloproteinases (TIMPs). This aberrant process of wound healing is known as fibrogenesis and associated with an increase of other ECM components such as lamins, proteoglycans and glycosaminoglycans[7]. Once liver regeneration fails and fibrosis proceeds by elevated ECM deposition[2], the risk to

develop HCC increases. Other important changes during advanced hepatic fibrosis are the loss of fenestrations of the liver sinusoidal endothelial cells (LSEC) and higher resistance to blood flow due to the high stiffness of MFBs. This causes hepatic insufficiency and portal hypertension which exacerbate liver injury[8].

In most cases, liver cirrhosis is the driver of HCC as this is an advanced chronic liver pathology showing nodules of regenerating hepatocytes which are in principle benign. However, over the time they can develop in dysplastic nodules which constitute pre-malignant lesions[8]. It is already accepted that cellular proliferation of injured hepatocytes and liver stem cells in a chronic inflammatory environment causes accumulation of genetic and epigenetic aberrations. This finally leads to malignant transformation and subsequently to early HCC[2] displaying a solid growth pattern with stroma and less frequently without tumor stroma[3]. Progression of HCC might be driven by hepatocyte replicative senescence underlying telomere shortening which impairs liver function[2]. Several stages of liver disease progression towards the establishment of HCC are represented in Figure 1.

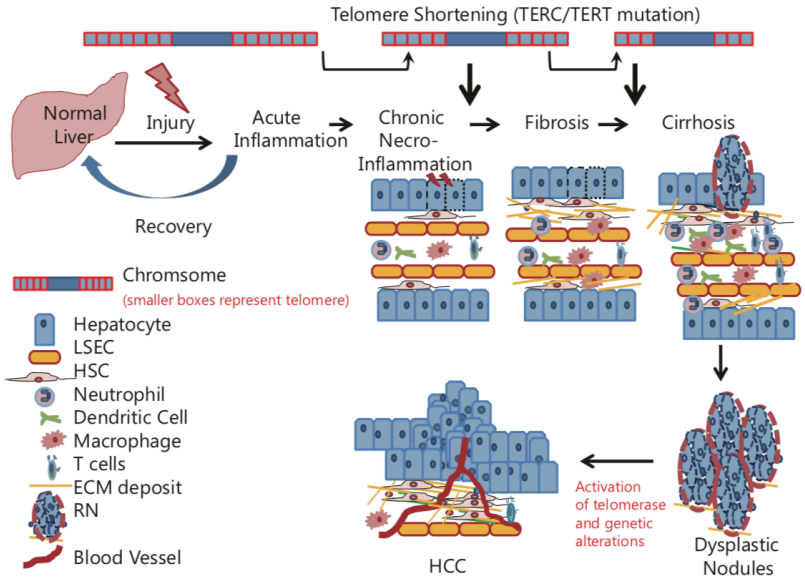

Figure 1. Scheme depicting several pathological stages during chronic liver disease progression towards HCC development. LSEC, liver sinusoidal endothelial cell; HSC, hepatic stellate cell; ECM, extracellular matrix; RN, regenerating nodule. Taken from Ramakrishna et. al.[2]

Among the genetic changes in HCC, TERT (telomerase reverse transcriptase) and c-Myc activations have been described to drive unlimited proliferation and malignant transformation of hepatocytes, respectively. In addition, activation of genes with metabolic and oxidative roles during early stages of HCC has been reported together with mutations of *i)* WNT/β-catenin signaling pathway, *ii)* p53, *iii)* HGF (Hepatic Growth Factor)/c-Met (its cognate receptor), *iv)* IGF (Insulin-like Growth Factor), *v)* EGFR (Epidermal Growth Factor Receptor) and *vi)* chromatin-remodeling proteins as well as *vii)* PI3K (Phosphatidylinositol 3-

Kinase)/Akt/mTOR (mammalian Target of Rapamycin), *viii)* Ras/Raf/MAPK (Mitogen-Activated Protein Kinase) and *ix)* Hippo/YAP signaling pathways[9]. Independent oncogenic aberrations cause in turn misbalance of the other signaling pathways, which furthermore amplifies the oncogenic transformation in a highly complex manner. One of the signaling pathways that is commonly affected by the above-mentioned mutations is the signaling network triggered by Transforming Growth Factor-β (TGF-β)[3].

There is a common feature among all types of cancer that also plays a significant role during HCC progression. In this sense, epithelial to mesenchymal transition (EMT) has shown to drive neoplastic transformation of hepatocytes and progenitor cells[10].

I.2 EMT and the role of TGF-β signaling pathway in HCC tumorigenesis and progression

EMT is one of the essential mechanisms during embryonic development[10]. This multistep, reversible and transient process is responsible for changes in the epithelial plasticity and differentiation stage of epithelial cells undergoing the transition. This mechanism plays a role during wound healing being beneficial but also in different deleterious pathologies such as fibrosis and cancer progression. EMT entails loss of cell-to-cell adhesion contacts and the apico-basal polarity of epithelial cells and gain of a mesenchymal-like phenotype characterized by a migratory and invasive behavior (Figure 2). This transition to a mesenchymal-like state is one of the first steps in the metastatic cascade allowing cells at the primary tumor front to locally invade and intravasate into blood and lymph, while cells of the main tumor bulk keep an epithelial character[11].

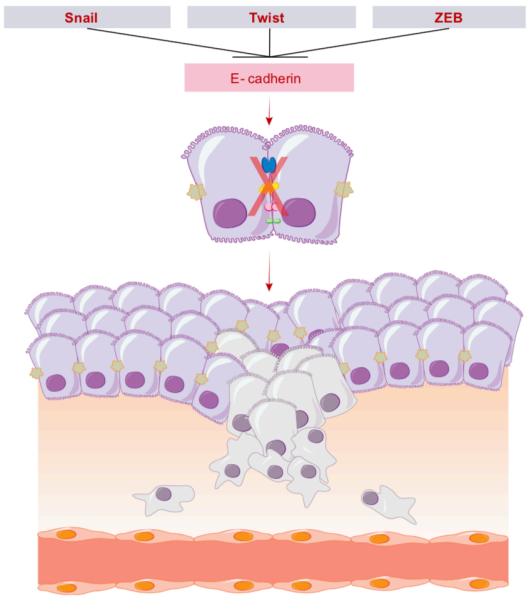

Figure 2. Scheme representing transcriptional repression of E-cadherin leading to EMT and HCC invasion. Adapted from Giannelli et. al.[6]

A hallmark of EMT is the loss of the adherens junctions between neighboring epithelial cells in which membrane-bound E-cadherin forms homotipic interactions with another E-cadherin molecule of an adjacent cell. In addition to the E-cadherin connection *per se*, the cytoplasmatic domain of E-cadherin interacts with β-catenin. α-catenin connects this heterodimer complex to actin filaments making the cell-to-cell junction more stable[12]. Furthermore, mesenchymal markers are upregulated during EMT including N-cadherin (involved in formation of plasma membrane

protrusions[13]), vimentin, α-SMA as well as direct and indirect transcriptional repressors of E-cadherin such as Snail1, Snail2, Zeb1, Zeb2 and Twist[6]. However, the specific EMT inducers and their cooperation to establish this state are signaling pathway-, tissue-, cancer type- and tumor stage-specific[10].

Changes in the epithelial plasticity towards a mesenchymal state is a transitional process, meaning that cells do not necessarily undergo a complete transition to a mesenchymal state but rather show a partial or hybrid phenotypes at different grades (Figure 3). At these transitional stages, the simultaneous expression of epithelial and mesenchymal markers is possible[11]. Furthermore, EMT is reversible and EMT-transformed cells can undergo a mesenchymal to epithelial transition (MET) which is believed to play a significant role in the seeding of circulating tumor cells in new target tissues[11]. In fact, EMT-MET cycles have been implicated in metastatic colonization of colon and breast primary tumors[6]. In this regard, it has been reported that fibrosis can be ameliorated by attenuation of EMT, which consequently promoted MET. Partial reversion of the fibrotic state was a result of targeting different EMT inducers[11].

Among EMT inducers, the zinc-finger transcription factor Snail1 has a crucial role as it represses E-cadherin by binding to E-box elements of its promoter, in contrast to Twist, which acts in an indirect manner. Snail1 is involved in development and cancer progression at onset of EMT, in contrast to other EMT transcription factors (EMT-TFs) which are expressed later to maintain the mesenchymal phenotype. In addition, Snail1 induces Snail2 expression in fibrosis and upregulates Zeb expression in carcinoma cells. Even though Zeb may also be expressed in Snail1-negative tumors, there is a hierarchy and cooperation among the EMT-TFs in which Snail1 is mostly the prominent inducer[10]. Interestingly, p53 activity causes the release of specific miRNA-mediated negative control of Zeb1 and Zeb2, thereby inducing EMT[6]. In fact, there is a plethora of miRNAs such as members of the miRNA-200 family that tightly tune the expression levels and functions of these EMT inducers. This regulatory machinery makes use of negative feedback loops between EMT-TFs and

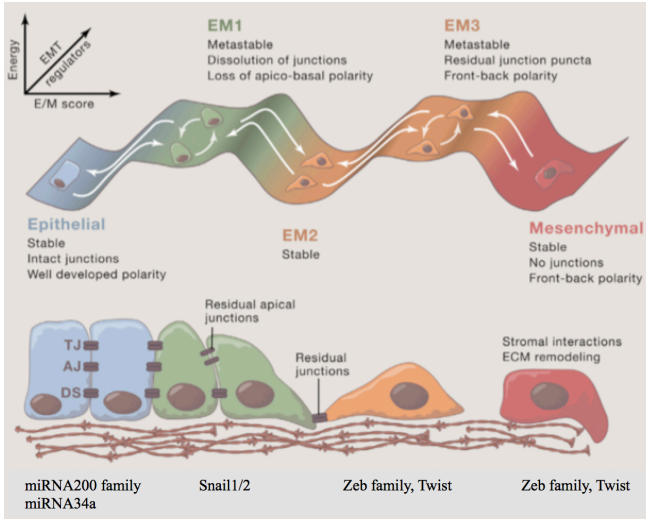

Figure 3. Cell plasticity through transitional states during EMT/MET. Adapted from Nieto et. al.[11]

between those transcription factors and the repressor miRNAs. Furthermore, protective transcription factors of the epithelial phenotype such as Ovol1/2 also exert a repressive activity on EMT inducers[11].

EMT is a highly conserved process and can be promoted by several factors including integrins, HGF, Fibroblast Growth Factor, PDGF (Platelet-Derived Growth Factor) and VEGF (Vascular Endothelial Growth Factor) as well as TGF-β[13]. In fact, TGF-β is implicated in EMT during embryogenesis and fibrosis in a process that entails de-differentiation in the case of the former. Likewise, TGF-β-induced EMT has been linked to carcinogenesis, even though this contrasts with the classical tumor-suppressor role attributed to TGF-β. However, it is already established that the TGF-β signaling pathway is a very complex network and plays a dual role during tumorigenesis depending on the tumor stage and the genetic context[14]. The tumor-suppressive functions of the TGF-β signaling are mediated by the canonical pathway leading to activation of cytostatic and apoptotic genes, which are observed in epithelial cells of healthy and adult tissues. TGF-β-mediated activation of the cyclin-dependent kinase inhibitors $p15^{Ink4B}$ and $p21^{Cip1}$ as well as repression of c-Myc and inhibitors of differentiation suppress proliferation, induce cell death and allow differentiation of epithelial tissues under physiological conditions[15]. In contrast, similar to the role that this cytokine is playing during embryogenesis and fibrosis, TGF-β signaling has been linked to EMT in combination with a defective genetic background that potentiates its tumor-promoting functions[14].

The TGF-β family is the largest human cytokine family whose members include three isoforms of TGF-β, activins, nodal, bone morphogenetic proteins (BMPs), growth and differentiation factors, all of them being essential during embryogenesis[15]. The canonical TGF-β signaling pathway is triggered by binding of the soluble cytokine to its membrane receptor, the dimeric form of type II TGF-β receptor (TGFBRII) which in turn recruits type I TGFBR (TGFBRI) for its activation via serine/threonine trans-phosphorylation (Figure 4). Once this heterotetrameric complex is formed, receptor-regulated Small Mothers Against Decapentaplegics (R-SMADs) proteins such as SMAD2 and SMAD3 are activated via TGFBRI-phosphorylation and translocate into the nucleus together with a common mediator, i.e. co-SMAD4. These heterodimeric complexes (SMAD2/SMAD4 or SMAD3/SMAD4) modulate the expression of TGF-β target genes in combination with other transcription factors. However, as in all transduction signaling pathways, there is a strict control of the cascade by negative regulation. Most notably among the negative controls at different levels, the negative feedback loop exerted by the inhibitory SMAD7 mediates the switch off of the canonical pathway by abrogating the activation of SMAD2 and SMAD3 by TGFBRI[7].

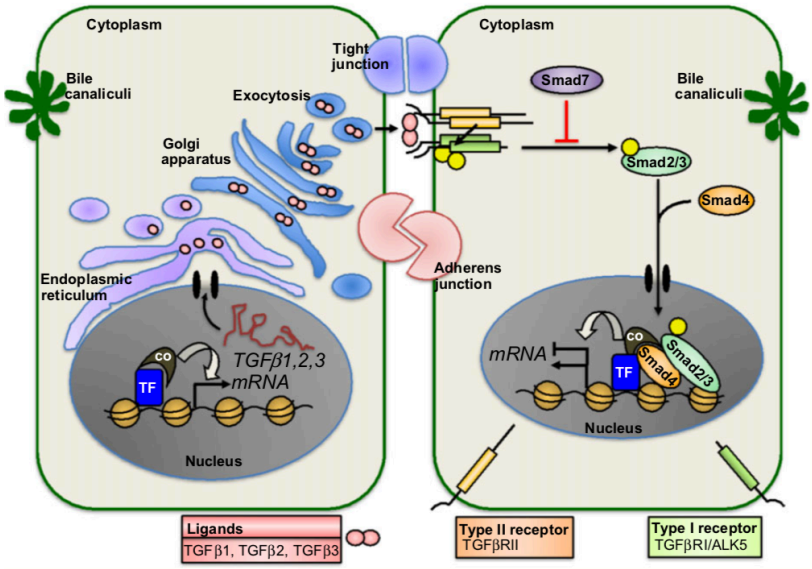

Figure 4. Scheme depicting the canonical TGF-β signaling pathway in two adjacent hepatocytes. Taken from Giannelli et. al.[7]

TGF-β has been involved in fibrosis, EMT and HCC progression. On one hand, upon hepatocyte injury, activated HSCs increase the secretion of this cytokine as compared to a healthy situation. TGF-β induces ECM deposition and modulates neighboring hepatocytes in an autocrine and paracrine modes of action, respectively. In addition, TGF-β increases focal adhesion and the mesenchymal marker α-SMA in HSCs[7]. Furthermore, a study has reported a reciprocal positive regulation between TGF-β and CD147, being the latter a glycosylated transmembrane protein expressed in activated HSCs and associated with cirrhosis[16]. These evidences highlight the role of this cytokine during hepatic fibrogenesis which is corroborated by a positive correlation between serum/liver levels of TGF-β and liver damage. In fact, there is a strong correlation between elevated TGF-β1 levels in the peripheral blood and HCC malignancy[7]. Translational studies have shown the positive benefits of targeting EMT using TGF-β inhibitors as a therapy against fibrosis[11].

Regarding EMT and carcinogenesis, it has been reported that hepatocytes undergoing this transition activate Akt and induce Extracellular Signal-Regulated Kinase (ERK)-1/2, which abolish the apoptotic effects of TGF-β and promote de-differentiation. A similar mechanism to escape apoptosis induced by long-term treatment with TGF-β was observed in hepatoblasts, which showed upregulated EGFR expression[7]. The synergism of this cytokine with other signaling pathways such as Ras/MAKP has also been reported to avoid cell cycle arrest and apoptotic events for induction of HCC progression[15]. In fact, the collaboration of these two signaling pathways drives upregulation of PDGF and its cognate receptor during EMT which in turn causes nuclear accumulation of β-catenin, a hallmark of self-renewal and proliferation[7]. In summary, TGF-β is a pleiotropic molecule whose signaling route has

crosstalk with many other signaling cascades at different levels leading to distinct pathophysiological outcomes.

It is noteworthy to mention that Snail1 and Snail2 are induced by the TGF-β superfamily members, being TGF-β1 the main inducer of Snail1 in different contexts[10]. This might explain why TGF-β-mediated tumorigenesis during early stages of HCC carcinogenesis in mice occurred by upregulation of Snail1 under different genetic backgrounds. Induction of HCC by genetic modification could be either by p53 silencing plus oncogenic $HRAS^{G12V}$ expression or by expression of oncogenic $HRAS^{G12V}$ plus oncogenic TAZ^{S89A}. Interestingly, this study demonstrated that TGF-β also displays a tumor-suppressive function *in vivo* upon expression of $HRAS^{G12V}$ plus c-Myc. The tumor-promoting role of TGF-β was driven by the canonical signaling pathway and upon expression of SMAD7, this effect was reverted by decreasing tumorigenesis in mouse livers.

The above-discussed research demonstrated that TGF-β functions are dependent on the genetic alterations. However, Snail1 seems to be a tumor inducer in hepatocytes, since ectopic expression of Snail1 in genetically engineered mouse livers ($HRAS^{G12V}$ plus c-Myc) caused an increase in tumorigenesis. This result was irrespective of the tumor-suppressive activity that TGF-β showed in that mouse HCC model. Notably, another study in pancreatic cancer revealed that TGF-β played a tumor-suppressive activity mediated by upregulation of Snail. Altogether these evidences suggest that Snail1 upregulation mediated by TGF-β leads to opposite outcomes during early stages of tumorigenesis depending on the type of cancer[14]. In addition, the last idea indicates that different tissues might respond to EMT inducers in different ways, undergoing either EMT or apoptosis. Therefore, the understanding of TGF-β effects requires taking into account the wide network of factors that modulate its function including cell type, genetic and epigenetic modifications, tumor microenvironment and tumor stage.

EMT and TGF-β have also been involved in hepatocellular stemness. Acquisition of stemness features as those shown by cancer stem cells (CSCs) is important since this potentiates cancer malignancy including enhanced dissemination and ability to form heterogeneous tumors in secondary sites[11]. In this sense, HCC cells upon TGF-β treatment and undergoing EMT have displayed a higher expression of the stem cell marker CD44. Likewise, EMT *per se* has been associated with other stemness markers[6]. However, EMT is not necessarily linked to stemness and these two processes in CSCs might occur in parallel but mediated by different pathways[11].

Stemness properties include self-renewal ability, which is directly linked to the WNT/β-catenin pathway by expression of c-Myc, cyclin D1 and other regulators of cell cycle progression[12]. In fact, nuclear accumulation of β-catenin in a complex with T cell factor (TCF) 4 leads to positive regulation of Snail1 and Snail2 expressions in HCC. Interestingly, a hepatic differentiation marker, HNF4α abolishes the upregulation of Snail genes via reduction of β-catenin expression levels during HCC progression. This mechanism regulates de-differentiation towards a mesenchymal phenotype as part of a double negative feedback loop that controls *in vivo* EMT in HCC[17]. Besides, WNT/β-catenin signaling also promotes Twist expression and downstream mediators of this signaling route control localization and stability of EMT-TFs leading to EMT[18]. Even more complicated, there might be a reciprocal and positive feedback regulation between EMT inducers and the above-mentioned signaling pathway. Loss of adherens junctions during EMT releases cytoplasmatic β-catenin from the E-cadherin/β-catenin complex. It might be expected that β-catenin translocates into the nucleus and activates the expression of EMT inducers. However, it is still unclear whether the β-catenin pool associated with E-cadherin has such a transcriptional contribution to the EMT program[18].

As discussed previously, EMT has been considered to be essential for metastasis initiation. However, the impact of EMT in all the steps of the metastatic cascade is controversial, even though EMT has been clearly implicated in conferring chemoresistance[11]. To fully understand how the metastatic process initiates and progresses until the establishment of a secondary tumor, it is fundamental to describe the whole mechanism step by step, the main drivers and the conditions needed for a successful tumor cell seeding in a new competent niche.

I.3 HCC metastasis: from tumor growth to pre-metastatic niche formation

Metastasis worsens the clinical control of cancer-related disorders. Whereas targeting primary tumors is still a challenge due to the diversity of cancers and individuals, metastatic outgrowth adds an extra layer of complexity for designing anti-cancer therapies. This is due to the fact that cancer cells localized in a primary site can disseminate and colonize more than a secondary organ. The parallel and the linear progression models suggest that metastasis might represent an early or late event during cancer development, respectively. Irrespective of these models, the metastatic cascade consists of several distinct steps such as i) local infiltration of tumor cells in the neighboring tissue, ii) intravasation, iii) survival in the circulation, iv) extravasation and v) seeding of the tumor cells either in proximal sites of the same organ or in distal organs, which are considered as the new "soil" or pre-metastatic niche[13] (Figure 5).

Establishment of a primary tumor needs oncogenic transformations and a suitable microenvironment that allows cancer cells to grow and expand. In this line, tumor-stroma

interactions in HCC are crucial among the transformed hepatocytes, HSCs, MFBs, LSECs and liver-homing immune cells as Kupffer cells. In addition, the tumor milieu is formed by recruitment of systemic immune cells to this site such as bone marrow derived-macrophages with a M2 phenotype, neutrophils, T and B lymphocytes and mesenchymal stem cells as well as endothelial cells forming the blood vessels[19]. In this context, M2-like macrophages and MFBs in the tumor stroma are called tumor-associated macrophages (TAMs) and cancer-associated fibroblasts (CAFs), respectively.

Secretion of soluble factors such as pro-inflammatory cytokines (e.g., IL-1, IL-6, TNF-α), chemokines, growth, pro-angiogenic and ECM-remodeling factors by the repertory of cells present in the tumor microenvironment is responsible for making the micro-niche fertile for tumor proliferation. Noteworthy, immune cells in the tumor niche switch from inflammatory to immunosuppressed phenotypes which impacts negatively on their anti-tumor activity. In fact, the presence of regulatory T (Treg) cells in the tumor microenvironment is a common event. Interestingly, these changes are mainly mediated by CAFs[19]. TGF-β is also an exceptional factor of the tumor-stroma interactions. Apart of promoting EMT and ECM remodeling by induction of matrix metalloproteinases (MMPs) such as MMP9[6], TGF-β also promotes production of the mitogenic PDGF in an autocrine manner and plays an immune-evasion function[13].

Angiogenesis stimulated by hypoxia and inflammation upon liver damage plays a critical role in supplying the exponential growing mass of transformed hepatocytes with oxygen and nutrients. Indeed, hypoxia promotes the expression of angiogenesis-promoting genes. Constant hepatic injury is associated with a strong and amplifying immune response, consequently, pro-angiogenic factors are secreted by immune cells. Those soluble factors attract endothelial cells which are the key components for the development of new blood vessels. The switch from physiological to pathological angiogenesis is partially mediated by VEGF and angiopoietins secreted by activated HSCs[20]. These cells also secrete mitogenic factors such as HGF which promotes hepatocyte proliferation and tumor growth[19].

As discussed above, HCC cells undergo EMT and by this mechanism are able to trans-migrate into blood and lymphatic vessels by passive and active processes. Active processes entail that circulating tumor cells (CTCs) are responsive to factors that allow them to enter the vasculature and migrate, for instance, following a gradient of growth factors and secreted chemokines. Once in the circulatory system, CTCs have to be able to survive and reach a new tissue after extravasation. In this regard, platelets have been reported to confer protection to CTCs against immune surveillance, high blood pressure and shear forces (Figure 5)[13]. On the other hand, CTCs express and secrete their own surface factors such as membrane-bound

tissue factor that helps them to survive during the migratory process by inhibiting coagulation and stimulating angiogenesis[13].

Concerning CTC migration through the systemic circulation, it has been published that those cells can migrate as independent mesenchymal-like cells or clusters as during embryogenesis, the latter displaying a higher metastatic potential[11]. Circulating clusters of tumor cells derived from melanoma and breast cancers retain some epithelial traits that allow them to have cell-to-cell connections to migrate collectively through capillary-sized vessels adopting a single-file chain-like reorganization for dissemination[21]. It has also been proposed that epithelial cells might intravasate and disseminate and there is a hypothesis suggesting that few mesenchymal-like cells and TAMs can help those epithelial cells during this process. Another important point that needs further studies is the definition at which stage of the metastatic cascade CTCs undergo a MET-like process. In principle, CTCs might reverse to a more epithelial character either before reaching the secondary tumor site, i.e. in the circulation, or after the metastatic seeding in the secondary tissues has started[11].

CTCs which are able to exit the circulation towards a permissive niche for seeding and proliferation show an advantage to avoid the adverse environment in the circulation and metastasize. Extravasation of CTCs represents a multi-step complex process with passive or active migration along the vessel, adhesion of those cells to the wall of the vessel lumen known as vessel arrest, and transendothelial migration. This process is not only dependent on the malignant potential of CTCs, but also on the specific characteristics of the local endothelium. This suggests a crosstalk between cancer cells and the vessel vasculature, whereby CTCs can reprogram endothelial cells[22].

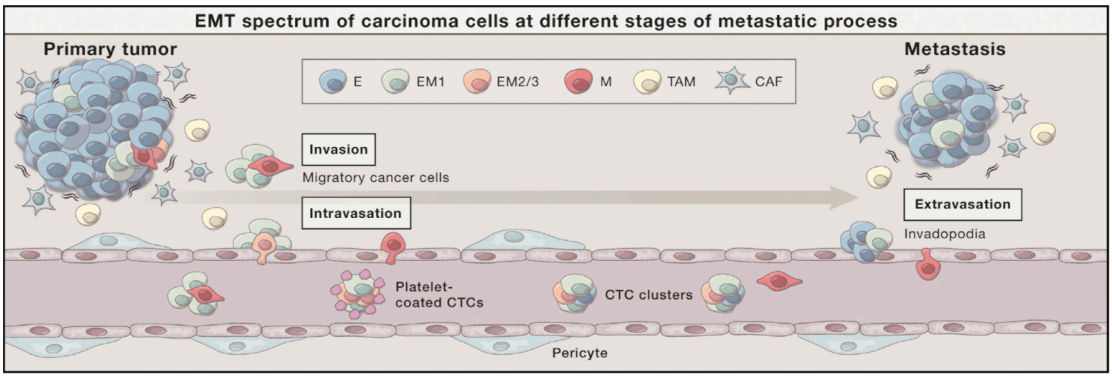

Figure 5. The metastatic cascade. E, epithelial cancer cell; EM1 and EM2/3 represent tumor cells undergoing progressive EMT but with a partial epithelial-mesenchymal state; M, mesenchymal tumor cell; TAM, tumor-associated macrophage; CAF, cancer-associated fibroblast. Taken from Nieto et. al.[11]

A study using human breast adenocarcinoma cells in a zebrafish model showed that Twist and VEGF-A are implicated in promoting a higher extravasation potential[22]. These authors

demonstrated that vasculature remodeling and endothelial cell clustering at the site of extravasation was β1-integrin dependent and enhanced by VEGF-A. Notably, a β1-integrin independent mode of extravasation was induced by Twist. The latter mode of action could be associated with transmigration through the endothelium in the absence of cell adhesion and in the presence of protrusions in the membrane of CTCs after an active intravascular migration of previously arrested cells[22].

Human cervical cancer cells have been shown to extravasate and adhere to the tissues surrounding the blood vessels. In this more recent study, clusters of cancer cells displayed two mechanisms for extravasation, i.e. active invasion by tranversing the wall of the blood vessel and endothelial covering. The latter refers to the covering of the CTCs attached to the blood vessel by a layer of endothelial cells. This event is followed by disappearance of the original endothelial layer of the vessel and release of the cancer cell cluster into the external tissue. This study suggested that cells in collective are able to extravasate as single cells do with the advantage of having higher chances to survive outside of the vessel, due to secretion of growth factors and signal molecules by each cell of the cluster. A dependency of the active invasion-like extravasation mechanism on VEGF expression was indicated. However, the existence of VEGF-independent extravasation mechanisms e.g., endothelial covering were proposed to explain the retention of the metastatic potential of cancer cells upon treatment with anti-angiogenic drugs targeting VEGF[23].

CTCs show an organotropism to metastasize, meaning that there are specific conditions in certain organs that allow those tumor cells to seed and colonize them. Indeed, the pre-metastatic niche generated by long-range signaling from the primary tumor is considered essential to support this organotropism. Primary tumor cells orchestrate the adaptation of the new target tissue by secretion of soluble factors that on one hand, directly reprogram the microenvironment of the metastatic site. On the other hand, those factors recruit bone marrow-derived cells (BMDCs) to further promote this process. Among these mechanisms, an essential event is the deposition of fibronectin which is upregulated by tumor-derived growth factors. In parallel, the hypoxic primary tumor secretes a lysyl oxidase into the circulation. These two proteins mediate the crosslinking of collagen IV which leads to adherence of already recruited MMP2-secreting BMDCs. Consequently, collagen IV is degraded allowing recruitment of more BMDCs and the incoming CTCs[24]. Prior to fibronectin deposition, primary tumor cells secrete VEGF-A, TNF-α and TGF-β which induce the initial recruitment of VEGF-R1-expressing BMDCs. This is followed by expression of inflammatory chemoattractants such as members of the S100A family to further recruit more myeloid cells before the arrival of CTCs[24]. In summary, primary tumor cells generate a new and sometimes

distal microenvironment that resembles the initial soil based on the inflammatory background and the ECM composition. Accordingly, angiogenesis might be induced in the new metastatic site by recruitment of VEGFR1 positive-BMDCs and VEGFR2-positive endothelial progenitor cells[24].

Even though the role of soluble factors such as growth factors, cytokines, chemokines and ECM remodelers is fundamental during pre-metastatic niche formation, those are not the only ones priming the new site for metastatic outgrowth. Tumor-derived exosomes (TDEs) are highly relevant in establishing the basis for micro- and macro-metastases. Exosomes are membrane-derived extracellular vesicles (EVs) formed in late endosomes and secreted by cells for horizontal transfer of information of different nature. In fact, the internal cargo of EVs can include DNA fragments, mRNAs, miRNAs, long non-coding RNAs, lipids, metabolites and proteins such major histocompatibility complex (MHC) class I and II, growth and transcription factors[25]. These vesicles are the smallest membranous particles secreted by cells with a diameter below 150 nm and a density between 1.13 and 1.19 g/mL[26]. The ability of carrying cellular molecules makes them suitable messengers to mediate cell-to-environment interactions, cell-to-cell communication, and depending on the context, those small vesicles can modulate signaling transduction pathways in recipient cells.

TDEs were initially implicated in mediating stromal-to-cancer cell interactions, blocking differentiation of myeloid cells, inducing immune suppression and transferring oncogenes. Besides, the amount of released vesicles correlates with the malignancy of the cancer cells[24]. Therefore, cancer research started a new era with exosomes that has extended the understanding of the multiple tumorigenic processes in which these vesicles are involved, with new possibilities to develop effective and targeted anti-cancer therapies. Thereby, TDEs have been demonstrated to collaborate with EMT during HCC progression.

I.4 Tumor-derived exosomes and metastasis

The first report describing the existence of membrane-derived vesicles which are secreted from late endosomes containing multivesicular bodies (MVBs) dates from 1983. Exosomes were recognized as vesicles shed from cells once the endocytic multivesicular compartment fuses with the plasma membrane, releasing the MVBs into the ECM and physiological fluids such as plasma, saliva, urine and breast milk. Exosome biogenesis has been proposed to follow an "inward-budding model" since these vesicles internalize cytosolic proteins into their cargo and display the same orientation of integral membrane proteins than those in the plasma membrane. However, they expose phosphatidylserine at the surface as in the reverse budding mechanism that drives the formation of most of the intracellular and plasma membrane-derived vesicles[27].

More than three decades ago, exosomes were reported as being part of the cellular mechanisms to release unwanted material from cells such as loss of the transferrin receptor during *in vitro* maturation of reticulocytes into erythrocytes[28]. More than 10 years later, exosomes were recognized as active biological entities involved in mediating cellular communication, specifically as intercellular messengers that are able to elicit an immune response. Besides, it was reported at that time that cells of hematopoietic origin as well as every cell with multivesicular endocytic compartments could secrete these small membrane-derived vesicles[27]. Up to date, three lines of evidence involve exosomes in EMT, pre-metastatic niche formation and immune escape together with modulation of immune cells to support metastasis[29].

TDEs carry EMT inducers and can promote changes in the epithelial plasticity of cells, which have uptaken these small extracellular vesicles (sEVs). In this sense, sEVs derived from highly metastatic human HCC cells have been shown to promote migration and invasion of non-motile immortalized human hepatocytes[30]. RNA profiling of exosomes isolated from those cell lines revealed that coding RNAs could be used to classify the parental cells according to their motile ability. In addition, there were differentially represented transcripts in sEVs derived from HCC cells as compared to those isolated from non-tumorigenic hepatocytes. Among the mRNAs and proteins uniquely and highly present in metastatic HCC cell-derived sEVs, S100A and caveolins as well as c-Met were identified, respectively. Therefore, exosomes acted as messengers for horizontal transfer of caveolins and c-Met proteins, which activated the MAPK and PI3K/Akt signaling pathways and subsequently, induced secretion of MMP2/9 by hepatocytes[30]. This study highlighted the significance of sEVs to mediate cell-to-cell communication for induction of tumor-associated behaviors. Moreover, functions of these vesicles and their specific cargo were dependent on the parental cells. In summary, this evidence might represent one of the strategies of HCC cells to promote their invasion by modifying the surrounding composed of healthy hepatocytes that start secreting ECM-degrading proteins via activation of c-Met-triggered signaling pathways (Figure 6).

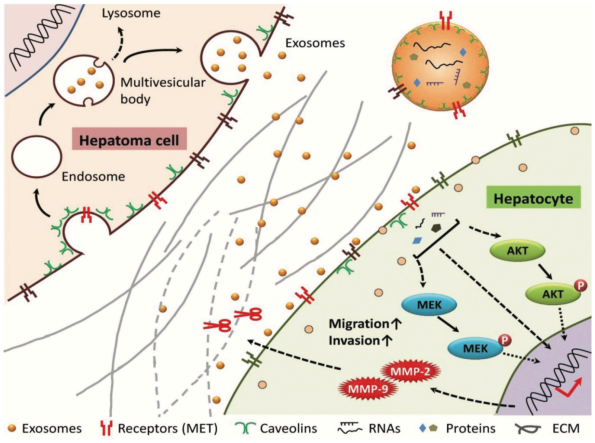

Figure 6. Schematic representation of the crosstalk between HCC cells and hepatocytes mediated by TDEs leading to enhanced migration and invasion of the healthy cells. Taken from He et. al.[30]

Interestingly, muscle-invasive human bladder cancer cells secrete sEVs that have shown to increase the transcript levels of mesenchymal markers such as α-SMA, vimentin, Snail, Twist and S100A4 in recipient primary urothelial cells. In addition, the sEV-treated urothelial cells expressed lower protein levels of E-cadherin and β-catenin and increased their migratory and invasive abilities. sEVs purified from those bladder cancer cells demonstrated chemoattractant properties leading to higher invasion of urothelial cells upon stimulus. This evidence clearly points out the involvement of sEVs in EMT[31].

sEVs secreted by prostate cancer cells upon hypoxia enhanced migration, invasion and stemness after treatment of naive cells. These effects were connected with an impaired expression of E-cadherin at the plasma membrane and an increase of cytoplasmatic and nuclear levels of β-catenin in the recipient cells. Hypoxic sEVs displayed a higher metalloproteinase activity relying on MMP2/9 and higher protein levels of β-catenin, Akt, TNF1-α, IL-6 and TGF-β2 when compared to vesicles secreted under normoxic conditions. Prostate stromal cells treated with those hypoxic sEVs showed higher expression of α-SMA, a marker of a CAF-like phenotype which is induced in these cells by TGF-β2[32]. This study demonstrated that upon hypoxia, a hallmark of tissue damage during tumor proliferation, secreted sEVs increased malignancy of both parenchymal as well as stromal cells. The phenotypic changes induced in these prostate cells resembled those occurring in EMT and during alteration of the healthy stroma surrounding tumor cells.

sEVs involved in acquisition of mesenchymal traits have also been described in nasopharyngeal cancer and mesothelial cells treated with breast cancer-derived vesicles[29]. Regarding exosomes and their contribution to the crosstalk between tumor and stromal microenvironment, four articles published between 2010 and 2015 reported that exosomal TGF-β is playing a role during differentiation of fibroblasts to myofibroblasts. One of these studies revealed that TGF-β associated with exosomes derived from prostate cancer cells activated a differentiation program in bone marrow-mesenchymal stem cells (BM-MSCs) that led to a myofibroblastic phenotype. These α-SMA-myofibroblast-like cells expressed higher levels of VEFG-A, HGF and MMPs. Furthermore, the differentiated BM-MSCs produced factors with pro-angiogenic effects which consequently induced tumor proliferation and invasion. Strikingly, a matched dose of soluble TGF-β1 did not show the same effects than those induced by the exosomal cytokine. Silencing of Rab27a in prostate cancer cells abolished the pro-invasive behavior of the tumor cells treated with exosome-differentiated BM-MSCs, confirming previous results which have suggested that this GTPase is involved in exosome secretion[33].

Other studies further demonstrated that differentiation to myofibroblast-like cells upon sEV stimulus is mediated by the canonical signaling pathway of TGF-β, more specifically by activation of SMAD3. This effect was dependent on heparan sulphate side chains of betaglycans (TGFBRIII) suggesting that exosomal TGF-β rather than being part of the vesicular cargo, is bound to the external surface of exosomes by this transmembrane proteoglycan. In that way, TGF-β is delivered to recipient cells in a biologically active form. In addition, sEV-treated stromal cells showed expression of the above-mentioned factors and a pro-angiogenic behavior similar to diseased stromal cells from prostate cancer patients. These stromal cells treated with TDEs increased tumor growth in xenotransplanted mice with prostate cancer cells[34]. Altogether these studies suggest that sEVs can modulate the stromal microenvironment leaving open the possibility of bio-nanoparticles acting in the local site as well as targeting distal organs.

Establishment of the vesicular traffic between cells entails that exosomes need to be uptaken by recipient cells. This process depends on the surface proteins exposed on those vesicles and the receptors present in the target cells. Likewise, organotropism is a critical determinant of exosome traffic during the pre-metastatic processes, which might be mediated by adhesion components, chemokine receptor/ligand partners and ECM proteins[29].

A recent study reported that education of mice with sEVs enhanced the metastatic potential of their parental tumor cells by modulation of the pre-metastatic niche *in vivo*[35]. Interestingly, cancer cells and their derived sEVs displayed the same organotropism. This effect also facilitated metastatic outgrowth of tumor cells with less affinity for the organ whereby exosomes derived from other cancer cells showed tropism. Lung-, liver- and brain-tropic sEVs showed differential expression of integrin (ITG) proteins, which mediated sEV adhesion in specific areas within the organs. ITG$\alpha_6\beta_4$ and ITG$\alpha_v\beta_5$ were essential for lung and liver metastasis *in vivo,* respectively. In particular, Kupffer cells in a fibronectin-enriched environment were targeted by liver-tropic exosomes derived from pancreatic cancer cells. As presented previously, members of the pro-migratory and pro-inflammatory protein family S100A were also upregulated in exosome-recipient cells in an exosomal integrin-dependent manner. Finally, this study proposed the use of specific exosomal integrins as predictive markers for metastatic organotropism of breast and pancreatic cancers[35].

Pancreatic ductal adenocarcinoma (PDAC)-derived sEVs were shown to increase liver metastatic burden *in vivo*. Adaptation of pancreatic cancer cells in the liver pre-metastatic niche was partially mediated by Kupffer cells once sEVs were uptaken by these macrophages. Consequently, TGF-β expression was increased in those liver immune cells. This led to activation of HSCs and subsequently, to a higher production of fibronectin by the activated

stromal cells. In this fibrotic context, bone marrow-derived myeloid cells such as macrophages and neutrophils were recruited. Macrophage migration inhibitory factor (MIF), a marker that was highly present in those TDEs was demonstrated to induce TGF-β expression in Kupffer cells and cause the activation of the fibrotic process. Furthermore, MIF protein levels in sEVs of PDAC patients' plasma correlated with liver metastasis in those individuals, suggesting the valuable use of MIF as a biomarker[36]. In a more recent study, activation of the above-described fibrotic process was accompanied by increased expression of S100A members and myeloid-derived suppressor cells (MDSCs) in peripheral blood of a mouse model of pancreatic cancer upon treatment with PDAC-derived sEVs. Altogether these changes enhanced primary tumor growth, liver pre-metastatic and metastatic processes upon sEV-mediated education of those mice[37].

Beyond pre-metastatic niche formation, TDEs have suppressive immune-modulation functions including induction of apoptosis of $CD8^+$ T cells, proliferation and recruitment of Treg cells, decrease of the cytotoxicity mediated by NK cells, inhibition of T helper 1 and 17 cell differentiation and antibody opsonization. However, positive immune modulation has also been reported based on the ability of TDEs to induce production of pro-inflammatory TNF-α and IL-6, a finding that was shown in lung metastasis[29]. A summary of the main functions of TDEs during tumor progression and metastasis according to above-mentioned evidences is represented in Figure 7.

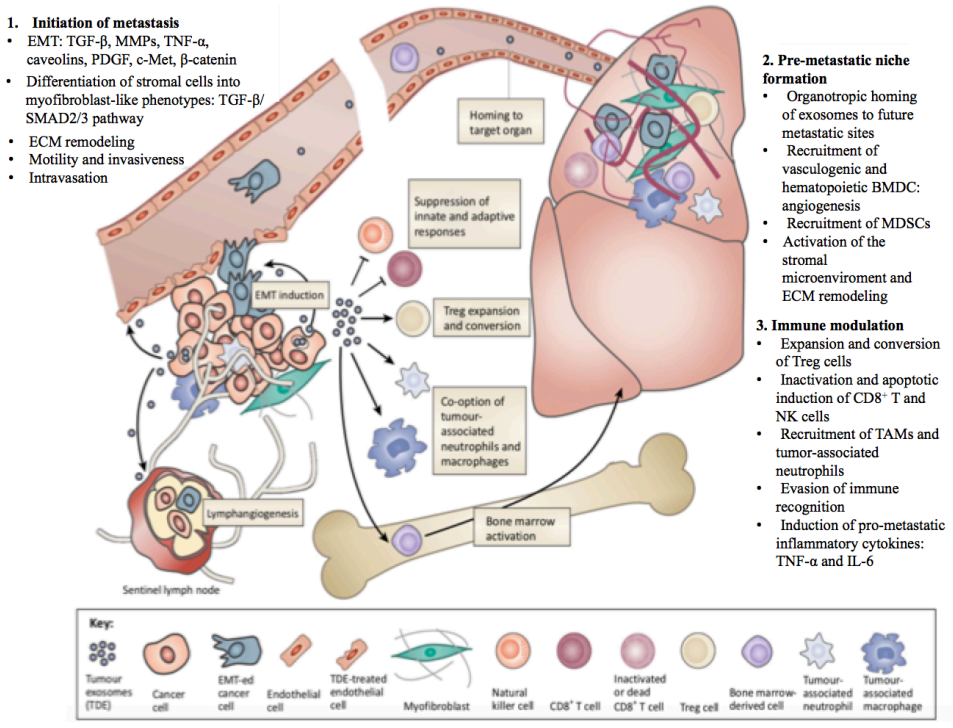

Figure 7. Three major functions of TDEs in tumor progression and metastasis. Adapted from Zyn et. al.[29]

Due to the ability of exosomes to circulate and target distal sites, these vesicles have been studied as a delivery system for anti-cancer targeted therapy. In this regard, engineered sEVs derived from mesenchymal cells and carrying on an RNA interference (RNAi) to target $KRas^{G12D}$, a common mutation driving PDAC development, suppressed tumor growth and increased mouse survival compared to RNAi-bearing liposomes. The advantage of using sEVs to target oncogenic KRas-expressing tumors was based on the presence of CD47 on the exosome surface. The glycosylated transmembrane protein inhibited phagocytosis and avoided rapid clearance of these biological messengers from the circulation[38]. Likewise, anti-cancer therapeutics might target TDEs based on drugs or compounds that decrease exosome biogenesis, secretion, uptake pathways or alter the internal cargo to reduce their pathological effects[29]. Finally, TDEs have also shown benefits in cancer diagnostics once detection of exosome markers in plasma/serum of cancer patients might be used as a liquid and non-invasive biopsy. This has been published for different types of cancer including breast, prostate, colorectal, ovarian, lung and pancreatic cancers as well as glioblastoma. Exosomal biomarkers such as proteins and nucleic acids, mainly miRNAs might be predictors of the cancer type and stage, and might additionally provide information about patient responses to anti-cancer therapies[25].

I.5 State-of-the-art isolation and characterization of exosomes

In last decades, there have also been progress concerning exosome purification and characterization. In first studies, "exosomes" were collected from reticulocyte supernatant by ultracentrifugation after those cells were grown in standard culture medium containing serum[28]. Later, a review published in 2002 pointed out that the standard procedure for exosome purification based on differential ultracentrifugation does not rule out the presence in the exosome pellet of other membrane-derived structures such as microvesicles and apoptotic bodies as well as large protein complexes. This means that a mixed population of different EVs might be co-isolated by this method. Therefore, a sucrose-based differential ultracentrifugation protocol was proposed to improve the purity of isolated exosomes together with a filtering step. In addition, the use of either serum-free or exosome-depleted serum was recommended when these vesicles are purified from cell culture conditioned medium. To determine size and shape of the isolated exosomes, the authors proposed electron microscopy[27].

Up to date, the gold standard methodology for exosomes purification is density gradient-based differential ultracentrifugation protocols. However, there is a large list of publications that indiscriminately performed different isolation protocols, meaning that differential ultracentrifugation approaches with and without a density gradient step are common in the

literature. Furthermore, the use of commercially available kits based on precipitation and membrane-affinity capture as well as immunoisolation, ultrafiltration and size-exclusion chromatographic methods have become very popular among the scientific community. Therefore, the field dedicated to study exosomes is rather heterogeneous from that point of view. Concerning EV detection, optical technologies for visualization, quantification and estimation of EV size have also been developed being Nanoparticle Tracking Analysis (NTA) one of the most used. NTA is based on light microscopy to detect and track particles in suspension showing a Brownian behavior. However, flow cytometry is also commonly used and adapted to detect these small particles[25].

Regarding the protein composition of sEVs, the presence of ubiquitous and cell-specific proteins has been reported in exosomes (Figure 8[39]). The most common ones are i) cytoskeletal proteins such as tubulin, actin and actin-binding proteins, ii) annexins and Rab proteins associated with intracellular membrane fusion and transport mechanisms, iii) proteins involved in the endosomal sorting complex required for transport (ESCRT) as tumor susceptibility gene (TSG)-101 and Alix, iv) metabolic enzymes and signal transduction molecules, v) proteins involved in antigen-presentation such as heat shock proteins (HSPs) and MHC I and vii) members of the tetraspanin protein family including CD9, CD63 and CD81. Among the proteins with cell-specific functions present in exosomes, transmembrane proteins such as integrins and immunoglobulins were reported and MHC II was described in antigen-presenting cell-derived exosomes[27].

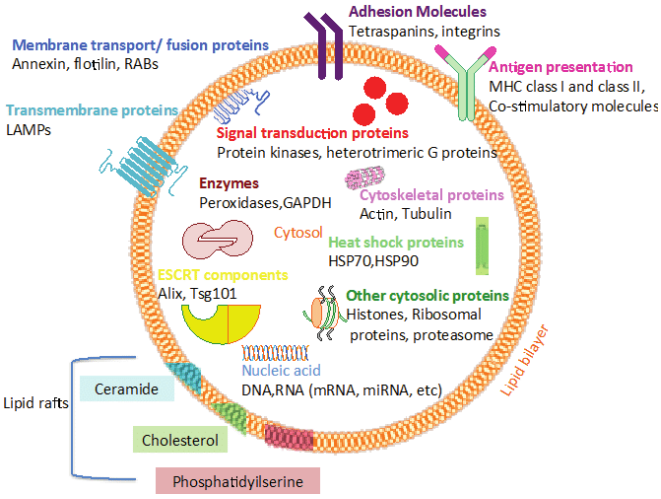

Figure 8. Scheme depicting the general molecular composition of exosomes. Taken from Garcia-Contreras et. al.[39]

A recent report showed that dendritic cell-derived EVs pelleted by differential ultracentrifugation at 10 000 x g (10K pellet) and 100 000 x g (100K pellet) presented common markers. Interestingly, those markers were classically believed to be specific for exosomes, the fraction of vesicles that pellets at the highest speed. For instance, the tetraspanin members CD9 and CD63 were enriched in the 100K-pelleted fraction but still present in the 10K pellet, meaning that tetraspanins *per se* are not specific of exosomes. In addition, flotillin-1, heat shock proteins and MHC I/II were not enriched in the 100K pellet,

suggesting that those proteins must not be used as specific markers either for sEVs or exosomes. As expected, an endoplasmatic reticulum protein (e.g., GRP94) was almost not detectable in both pellets but present in the whole cell lysate and in the pellet containing large EVs (2 000 x g, 2K pellet)[26].

Strikingly, these authors showed the advantages of adding the 100K pellet at the bottom of an iodixanol density gradient for a short-term floatation/ultracentrifugation step to isolate different subpopulations of sEVs. The light sEV-subpopulation (1.115 g/mL) contained the highest percentage of particles between 50 and 150 nm among the 100K pellet and the heavier sEV-fraction obtained after ultracentrifugation of the 100K in the density gradient. Regarding the tetraspanin enrichment, the light fraction showed higher levels of CD63. However, these subpopulations were hardly separated using a sucrose-gradient. The above-mentioned light fraction was enriched with TSG101, among other plasma membrane and endosomal proteins compared to the heavier fraction. It was also shown that within the 100K pellet recovered by ultracentrifugation, there was a more restricted subpopulation of sEVs containing CD63 compared to CD9 and CD81-bearing small vesicles. However, all CD63-bearing sEVs also contained the other tetraspanin members[26].

In summary, it has been proposed that exosomes are characterized by CD9/CD63/CD81 co-enrichment. However, depending on the cell type, the presence and relative abundance of all of them can vary. The presence of tetraspanin members together with TSG101 and syntenin-1 and the lack of endoplasmatic reticulum proteins was suggested as the most specific protein composition that can be use to detect exosomes[26]. However, beyond the isolation methods and exosome detection by protein markers, it has been demonstrated that mouse melanoma cells release different subpopulations of TSG101 and Alix-positive exosomes with specific size, density, RNA and protein composition. Exosome subpopulations derived from those cells displayed different biological functions in recipient cells. Furthermore, a wide range of cells such as mouse heart endothelial cells, immortalized mesenchymal stem cells as well as mouse neuroblastoma and human squamous carcinoma cells were also shown to export distinct exosome subpopulations similar to those secreted by melanoma cells[40].

In general, there has been a high level of discrepancy concerning protocols for exosome isolation and the particular markers for specific detection of those sEVs. For that reason, inconsistencies in the size and density values reported for exosomes can be found in the literature. Currently, several studies in this field have indicated the gold standard approaches that can be followed in order to increase the purity of exosomes and improve their characterization and unique detection using a combination of protein markers as those above-mentioned. However, there is still no consensus concerning these issues and optical

methodologies that are available for estimation of EV size and particle quantification show several limitations. Further studies will help to establish deeper knowledge about exosomes and their unique features, making this research field a more powerful tool to fight against cancer.

I.6 Hypothesis and aims

This project hypothesized that EVs have an impact on the epithelial plasticity of human HCC cells. In particular, we postulated that HCC cells displaying an epithelial phenotype might show a downregulation and upregulation of the mRNA levels of epithelial and mesenchymal markers, respectively, upon treatment with EVs derived from EMT-transformed HCC cells.

The use of the general term "extracellular vesicles, EVs" has been preferred according to the isolation protocol used in the present study resulting in co-isolation of sEVs and larger-sized bioparticles.

In order to verify this hypothesis and make some progress for further studies, several tasks were performed as described below:

1. Isolation of EVs derived from HCC cell lines showing an EMT-transformed phenotype (HLF, HLF-T and SNU449 cells) by differential ultracentrifugation and a membrane affinity-based commercial kit. Characterization of these EVs by NTA and immunoblotting.
2. *In vitro* treatment of the epithelial HCC cell line HepG2 with EVs derived from HLF and HLF-T cells and analysis of the mRNA expression levels of epithelial and mesenchymal markers.
3. Generation of GFP-tagged CD63-expressing HCC cell lines (HLF and SNU449) for production of GFP-labeled EVs as a tool for further *in vivo* experiments. EV education of immunodeficient mouse models prior to xenotransplantation of HCC cells will be a future research project in order to study the involvement of EVs in HCC progression and pre-metastatic niche formation.

II MATERIALS AND METHODS

II.1 Cell lines and cell culture conditions

Human HCC cell lines including HepG2, HLF, HLF-T and SNU449 were split every two days and kept in culture up to three months. All of them were cultured in Dulbecco's Modified Eagle Medium (DMEM) at 37°C and 5% CO_2, except SNU449 cells which were cultured in RPMI-1640 medium. Both cell culture media were supplemented with 10% fetal

calf serum (FCS) and antibiotics (50 U penicillin (P) and 50 µg/mL streptomycin (S)). HepG2 cells were seeded in 10 cm-culture plates coated with 0.05 mg/mL type I-rat tail collagen.

HLF-T cells were obtained by long-term TGF-β1 treatment (1 ng/mL) of HLF cells (Haider C. et. al., 2018, manuscript in preparation). After the initial 10 days of TGF-β1 treatment, HLF-T cells were used for EV isolation. HLF-T cells were kept in culture for the maximum of 1 month after starting the TGF-β1 treatment. The cell culture medium was continuously supplemented with TGF-β1 once cells were split.

II.1.1 Scratch assay of HLF-T cells

To confirm the migratory abilities of HLF-T cells as compared to parental HLF cells, scratch assays were carried out after the initial 10 days of TGF-β1 treatment. Once the higher migratory phenotype of HLF-T cells was confirmed, these cells were used for further experiments such as EV isolation for treatment of HepG2 cells. For scratch assays, HLF and HLF-T cells (each 5 x 10^5 cells) were seeded in a 6-well culture plate. In a step before, vertical lines were drawn every 3 mm on the outer bottom of the wells to make easier and accurate image capture by microscopy and quantification of the migration rate, respectively. Horizontal scratches in the cell monolayer were made 24 hrs post-seeding with a 1 mL pipette tip (2 per well) and culture medium was replaced with a fresh one to remove detached cells. At this point (0 hr-scratching) and 24 hrs post-scratching, images were captured by microscopy (Nikon Eclipse Ti-S/L100, Japan; Imaging software, NIS-Elements version 4.30.01). Cell migration was analyzed by quantifying the gap area of 0 hr- and 24 hr-scratches (A_0 and A_{24}, respectively) by ImageJ 1.44p software. Relative cell migration of HLF-T cells was expressed as a normalized value respect to parental cells.

II.2 EV isolation from cell culture conditioned medium of HCC cell lines

The isolation of EVs was performed by differential ultracentrifugation (DUC) as described previously[41] (Figure 9). For a more detailed description, 12 x 10^6 - 21 x 10^6 cells (depending on the cell line) were seeded in 15 cm-tissue culture plates (Table 1). Culture medium was removed 24 hrs post-seeding and cells were washed three times with phosphate-buffered saline (PBS) followed by addition of FCS-free culture medium at the half of the volume usually used for cell seeding. After 24 hrs of cell growth in FSC-free medium, cell culture conditioned medium (CCM) was collected and centrifuged at 400 x g and 4°C for 10 min to pellet dead cells. Supernatant was filtered with a 0.22 µm cellulose acetate membrane-filter (Sartorius Stedim, Biotech, USA) to remove cellular debris and apoptotic bodies. Filtered supernatant was transferred to ultracentrifuge tubes (ultra-clear, thinwall 14 x 89 mm, Beckman Coulter) and centrifuged at 100 000 x g, 4°C for 90 min (SW41 Ti rotor, Optima L-100 XP Ultracentrifuge, Beckman Coulter, USA). Supernatants were discarded and pellets

were resuspended in cold sterile-filtered DPBS (Dulbecco's PBS, Sigma Aldrich, USA) and pooled to carry out a second ultracentrifugation step under the same conditions. The EV pellet was resuspended in 100-200 µL cold PBS and stored at -80°C.

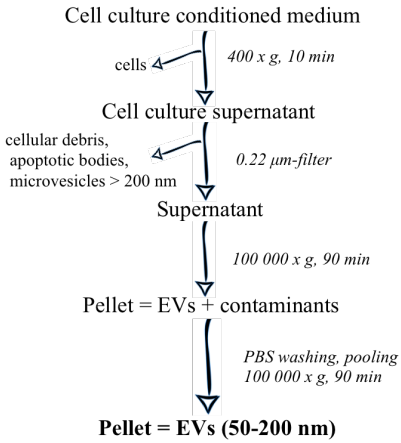

Figure 9. Flow chart of EV isolation from CCM by differential ultracentrifugation.

Alternatively, EVs were also isolated using a membrane-based affinity kit (exoEasy Maxi kit, Qiagen, Netherlands). The protocol was performed essentially as described by the manufacturer, except the filtering step in which a 0.22 µm filter was used instead of the indicated pore size (0.8 µm). EV samples consisted of eluted vesicles in an inorganic salt based-aqueous buffer (400 µL).

Table 1. HCC cell lines used for EV isolation from CCM

HCC cell line	***Cell number per 15-cm culture plate (x 10^6 cells)***	***FCS-free CCM volume (mL)***
HLF	18	12
HLF-T	12	12
SNU449	21	12

II.2.1 Estimation of EV concentration and size by Nanoparticle Tracking Analysis

EV samples were analyzed by NTA (NanoSight NS500, Malvern, UK) with a 532 nm-laser and with the following settings: detection threshold 5, camera level 14 and screen gain 1 (NTA 3.1 software). The standard operating procedure included six image captures (30 sec each) per sample. Sample dilution in PBS (1:200-1:500) was adjusted to measure a range of 1 x 10^8 - 1 x 10^9 particles/mL (corresponding to 10-100 particles per frame). PBS was measured as blank. Particle concentration and size were reported as mean ± standard error. Size distribution plots were constructed by gating the NTA measurement (1-1000 nm) at three different size ranges: < 150 nm, 150-200 nm and > 200 nm.

II.3 Western blotting for detection of EVs

EVs samples resuspended in PBS were lysed in RIPA buffer (PBS:RIPA, 1:1 (v/v)) with a freeze/thaw cycle at -20°C. EV protein concentration was quantified using a Micro BCA Protein Assay kit (Thermo Fisher Scientific, USA). Cells were lysed in RIPA buffer with a protease inhibitor cocktail, snap-frozen and after thawing up on ice, cell lysates were centrifuged (9 600 x g, 10 min, 4°C) to pellet the insoluble fraction. Protein concentration of cell lysate supernatant was determined by Bradford assay (Protein Assay Dye Reagent Concentrate, BioRad, USA).

Western blot samples were prepared in sodium-dodecylsulfate (SDS)-loading buffer 5X (250 mM Tris-HCl pH 6.8, 10% SDS, 5% β-mercaptoethanol (β-ME), 100 mM dithiothreitol (DTT), 3 mg/mL bromophenol blue, 30% glycerol). For detection of antibodies under non-reducing conditions, Western blot samples were prepared in a β-ME/DTT-free SDS-loading buffer. Samples were heated at 95°C for 5 min and cooled down on ice previous to SDS-polyacrylamide gel electrophoresis (SDS-PAGE).

SDS-PAGE was performed using 1 mm-thick gels (10 and 12% polyacrylamide) in the electrophoresis buffer (25 mM Tris, 192 mM glycine, 0.1% SDS) at 25 mA. Equal protein amount of EV and cell lysates were loaded onto the gel together with a pre-stained protein ladder with fragments between 10 and 250 kDa (PageRuler Plus Prest., Thermo Fisher Scientific). The sandwich mode-blotting (100 V, 1 hr) onto a nitrocellulose membrane (Amersham Protran 0.2 µm, GE Healthcare Life Science, USA) was performed in a cold blotting buffer (25 mM Tris, 192 mM glycine, 15% methanol, 0.02% SDS) and Ponceau staining (0.1% Ponceau S in 5% acetic acid) of the membrane was carried out prior to 1 hr-blocking step in either 4% bovine serum albumin (BSA) or 5% milk consisting of TBS-T (0.1% Tween-20 in TBS [20mM Tris, 150 mM NaCl, pH 7.5]). Blocking with BSA or milk was depending on the primary antibody. Primary antibodies for detection of EV markers as well as a negative EV marker and a housekeeping protein are listed in Table 2.

Table 2. Primary antibodies for detection of EV markers, a negative EV marker and a housekeeping protein.

Antibody	***Source and clonality***	***Clone***	***Dilution and conditions***	***Expected band (kDa)***	***Company***
CD63	mouse monoclonal	TS63	1:1000, 4% BSA in TBS-T/ non-reducing	30-60	Abcam, UK
CD81	mouse monoclonal	JS-81	1:250, 5% milk in TBS-T/ non-reducing	26	BD Pharmingen
TSG101	mouse monoclonal	C-2	1:100, 5% milk in TBS-T/ reducing	45	Santa Cruz, USA
GRP78	mouse monoclonal	40/BiP	1:500, 5% milk in TBS-T/ reducing	78	BD Transduction Laboratories
actin	rabbit polyclonal		1:2000, 4% BSA in TBS-T/ reducing	42	Sigma-Aldrich

Incubation with the primary antibody was perfomed overnight at 4°C, followed by washing three times with TBS-T buffer every 15 min. Peroxidase-labeled horse anti-mouse and goat anti-rabbit secondary IgG antibodies (1:1000, Vector Laboratories Inc, USA) were incubated at room temperature (RT) for 1 hr followed by washing three times with TBS-T buffer every 15 min. Developing of the blotted membranes was performed with Enhanced ChemiLuminiscence (ECL) reagent using H_2O_2 as the substrate and exposition to an X-ray film. For most of the antibodies, the ECL Select Western Blotting Detection Reagent

(Amersham, GE Healthcare Life Science) was used with an incubation step for 5 min. For detection of CD63 and actin, a self-made ECL reagent based on luminol/coumarin (0.1 M Tris pH 8.8, 13.07 mg/L para-coumaric acid in DMSO, 44.3 g/L luminol in DMSO) and 3% H_2O_2 (3 µL per mL of working solution) was used and incubated on the membrane for 1 min.

II.4 Treatment of HepG2 cells with mesenchymal HCC cell-derived EVs

HepG2 cells were seeded in a 12-well tissue culture plate with 0.9 mL DMEM supplemented with 10% FCS and P/S. As positive controls, HLF and HLF-T cells were seeded using the same cell number as for HepG2 cells. Single treatments of HepG2 cells with EVs isolated from HLF and HLF-T cells were performed for 24 and 72 hrs. Seeding density for 24 hr- and 72 hr-treatment was 7.5 x 10^4 and 5 x 10^4 cells, respectively. EV treatments for 24 hrs and 72 hrs were carried out in one experiment with duplicates and in three independent experiments with a replicate per sample, respectively. HepG2 cells were treated 24 hrs post-seeding with approximately 2 x 10^5 particles per cell (corresponding to roughly 0.3 ng of EV proteins/cell). After 24 hrs and 72 hrs of EV treatment, RNA was extracted from PBS- and EV-treated HepG2 cells as well as HLF and HLF-T cells.

All cells used in this *in vitro* experiment were seeded in additional 12-well culture plates for cell counting (CASY TTC Model cell counter and analyzer, Schärfe System, Germany) every day in order to control that cells were growing at exponential rate during the experiment period.

II.5 RNA extraction, reverse transcription and Real Time quantitative-Polymerase Chain Reaction (RT-qPCR)

RNA extraction was carried out using an RNeasy Mini kit (Qiagen, Netherlands). The protocol was performed as described by the manufacturer. In summary, cells were washed with ice-cold PBS and were scraped from the 12-well culture plate in the presence of a lysis buffer (300 uL of a denaturing guanidine-thiocyanate–containing buffer). Cell lysates were transferred to 1.5 mL microcentrifuge tubes and homogenized by passing more than five times through a blunt 21-gauge needle (0.8 mm diameter) and subsequently mixing the suspension with an equal volume of nuclease-free 70% ethanol to provide appropriate binding conditions. The mixture was transferred to a microspin column (silica-based membrane) and centrifuged at >8 000 x g for 15 sec. The flow-through was discarded and two buffers were sequentially added with centrifugation steps in-between to efficiently wash contaminants away. RNA was eluted with nuclease-free ddH_2O (30 µL) added directly to the spin column membrane. RNA concentration was measured by spectrophotometry (NanoDrop ND-1000, PeqLab, Germany).

Reverse transcription was performed according to the manufacturer specifications (QuantiTect Reverse Transcription kit, Qiagen, Netherlands) (Table 3) followed by measuring the cDNA concentration by spectrophotometry (NanoDrop ND-1000, PeqLab, Germany). The RT-qPCR reaction was performed with a SYBR Green-containing master mix (GoTaq qPCR Master Mix, Promega, USA) as described in Tables 4 and 5. Relative transcript levels of epithelial and mesenchymal markers were quantified considering RPL41 and PBS-treated HepG2 cells as the internal and negative controls, respectively (see primers and DNA sequences in Table 6). Relative mRNA expression was plotted after normalization with respect to the negative control.

Table 3. Reverse transcription reaction

step	***Component***	***Volume (µL)***	***Protocol specifications***
1	gDNA Wipeout Buffer 7X	2	Incubation (42°C, 2-8 min)
	RNA template	equivalent to 1 µg	
	RNase-free ddH_2O	variable	
	Total volume	14	
2	Quantiscript Reverse Transcriptase 7X	1	Preparation of the Reverse Transcription master mix and addition (6 µL) to each RNA sample Incubation at 42°C for 15-30 min followed by inactivation at 95°C for 3 min
	Quantiscript RT Buffer 5X	4	
	RT Primer Mix	1	
	Total volume (uL)	20	

Table 4. RT-qPCR reaction set-up

Component	***Volume (µL)***	***Final concentration***
GoTaq qPCR Maxter Mix 5X	5	1X
forward and reverse Primer Mix	2	200 nM (each primer)
cDNA template	2	20-50 ng
nuclease-free ddH_2O	1	
Total volume (uL)	10	

Table 5. RT-qPCR program

step	***Temperature (°C)/Duration (min)***	***Cycles***
Initial denaturation	95 / 2 min	
Denaturation	95 / 10 sec	40
Anneling/Extension	60 / 30 sec	
Melting curve	65-95 (0.5°C/0.05 sec)	

Table 6. Primer DNA sequences of the housekeeping and target genes

Gene		***Primer sequence***	***Company***
RPL41	forward	CAAGTGGAGGAAGAAGCGA	VBC Biotech
	reverse	TTACTTGGACCTCTGCCTC	
e-cadherin (CDH1)	forward	ACC ACC TCC ACA GCC ACC GT	Sigma-Aldrich
	reverse	GCC CAC GCC AAA GTC CTC GG	
SNAI1	forward	CCAGTGCCTCGACCACTATG	VBC Biotech
	reverse	CTGCTGGAAGGTAAACTCTGG	
SNAI2	forward	TGACCTGTCTGCAAATGCTC	VBC Biotech

Gene		***Primer sequence***	***Company***
	reverse	CAGACCCTGGTTGCTTCAA	
ZEB1	forward	TTACCAGGGAGGAGCAGTGA	VBC Biotech
	reverse	CCTTCCTTTCCTGTGTCATCCT	
ZEB2	forward	GCC GAG TCC ATG CGA ACT	Sigma-Aldrich
	reverse	AAT GAA GCA GCC GAT CAT GG	
TWIST	forward	TTCTCGGTCTGGAGGATGGA	VBC Biotech
	reverse	AATGACATCTAGGTCTCCGGC	
n-cadherin (CDH2)	forward	CCACCTTAAAATCTGCAGGC	VBC Biotech
	reverse	GTGCATGAAGGACAGCCTCT	
vimentin (VIM)	forward	ATTCCACTTTGCGTTCAAGG	VBC Biotech
	reverse	CTTCAGAGAGAGGAAGCCGA	

Read-out data (CFX96^{TM} Real-time System thermal cycler, BioRad, USA) were processed with the software supplied by the company (Bio-Rad CFX Maestro 1.0, version 4.0.2325.0418). Melting curves were analyzed to control primer specificity, primer dimer formation and contaminations.

II.6 Generation of HCC cell lines producing GFP-labeled EVs

HLF and SNU449 cells were transduced with a lentiviral vector coding for a CD63-GFP fusion gene. The lentiviral vector bearing the CD63-GFP construct (pLVX-CD63-GFP plasmid with a size of approximately 8900 bp) was a kind gift from Paola Martinelli and Sonia Melo (University of Texas MD Anderson Cancer Center, Houston, Texas, USA)[42].

pLVX-Puro vector (Clontech, USA) an HIV-1-based lentiviral expression vector was used as the backbone plasmid for restriction-based cloning of the fusion gene (CD63-GFP) downstream of the active human cytomegalovirus immediate early promoter ($P_{CMV\ IE}$, located just upstream of the multiple cloning site, MCS) (Fig. 10). As resistance markers, pLVX-Puro vector contained a puromycin resistance cassette (Puro^{r}) (under the control of the murine phosphoglycerate kinase (PGK) promoter (P_{PGK})) for selection of transduced cells. In addition, ampicillin resistance gene (Amp^{r}) was present for selection in bacteria. A pUC origin of replication for bacteria allowed propagation of the plasmid in transformed *E. coli* bacteria.

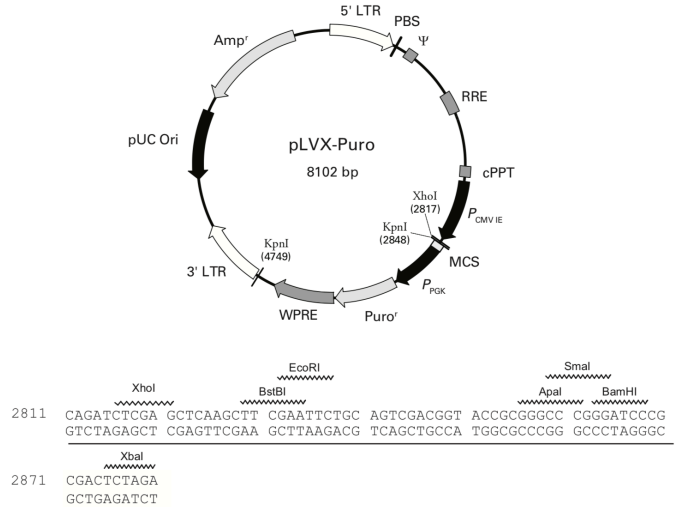

Figure 10. pLVX-Puro vector map and the multiple cloning site (MCS). Taken from Clontech, USA.

pCMV6-CD63-GFP (RG217238, Origene, USA) was the original plasmid bearing the GFP-tagged CD63 construct which was subcloned into the lentiviral backbone for constitutive expression of the fusion protein in recipient cells.

All the steps described below for generation of CD63-GFP-expressing HLF and SNU449 cells were carried out by ***Heidemarie Huber***, a member of the laboratory.

II.6.1 Heat-shock transformation of chemically competent bacteria with pLVX-CD63-GFP plasmid for propagation

CaCl-competent Sbtl3 *E. coli* bacteria stored at -80°C were thawed up on ice and 100 µL of bacteria were mixed with 100 ng of plasmid DNA in a pre-cooled microcentrifuge tube (expected efficiency ~ 1 x 10^8 transformants/µg of DNA). Competent bacteria/DNA mixture was incubated on ice for 20-30 min previous to heat shock transformation for 50 sec at 42°C and cooling on ice for 3 min. Meanwhile, 4°C-stored agar plates were warmed up as well as antibiotic-free Luria Bertani (LB) medium at 37°C. LB medium, 500 µL (10 g/L NaCl, 10 g/L tryptone, 5 g/L yeast extract) was added to bacteria for growing in a shaking incubator at 37°C for 60 min. Afterwards, bacteria were centrifuged at 18 800 x g, 4°C for 1 min, the supernatant was discarded and the bacterial pellet was resuspended in the remaining supernatant volume previous to plating onto 10 cm-LB agar plates (20 g/L agar) containing ampicillin (100 µg/mL). Plated bacteria were incubated overnight at 37°C.

A single cell clone was picked and inoculated in 5 mL LB-Ampicillin (LB-Amp) medium and pre-cultured overnight by shaking at 37°C. Pre-cultured bacteria, 10 µL were inoculated in 100 mL LB-Amp medium and cultured for 24 hrs.

II.6.2 pLVX-CD63-GFP plasmid purification from E. coli bacteria and restriction enzyme analysis

Plasmid DNA purification was performed by a Qiafilter plasmid Midi kit (Qiagen, Netherlands) from 100 mL of bacterial culture in LB-Amp medium. Briefly, the bacterial culture was harvested and the pellet was mixed with the Resuspension buffer (6 mL) containing LyseBlue reagent (1:1000) previous to add the alkaline Lysis buffer (6 mL). The mixture was incubated for 5 min at RT and 6 mL of Neutralization buffer was added. The final mixture was poured into a cartridge and the cell lysate was filtered into a pre-equilibrated Qiagen-tip. The bacterial lysate entered the anion-exchange resin by gravity flow and three washing steps with 10 mL of Washing buffer were carried out previous to DNA elution with 5 mL of a high-salt buffer into a centrifuge tube. DNA concentration and desalting were performed by DNA isopropanol precipitation (3.5 mL, RT) and ultracentrifugation at 15 000 x g for 30 min. DNA pellet was washed with nuclease-free 70%

ethanol (2 mL) followed by ultracentrifugation (15 000 x g, 10 min). In the last step, the DNA pellet was air-dried for 5-10 min and dissolved in 150 µL of nuclease-free ddH_2O at 37°C for 1 hr.

As control, purified plasmid DNA was digested at 37°C for 5 min with restriction enzymes such as BspHI and PmlI (FastDigest, Thermo Fisher Scientific) cutting each of them at two DNA sites within the plasmid (Table 7). The digested, linearized (by BamHI) as well as the undigested plasmid were loaded onto a 1.5% agarose gel together with a DNA ladder (GeneRuler 100 bp Plus, Thermo Fisher Scientific). Selection of the restriction enzymes for digestion and linearization of the plasmid was done using SnapGene Viewer 4.0.

Table 7. Digestion with restriction enzyme set-up

Component	***Volume (µL)***
FastDigest Green buffer 10X, (Thermo Fisher Scientific)	7
FastDigest restriction enzyme	1
Plasmid DNA	1 (up to 0.5 µg)
nuclease-free ddH_2O	1
Total volume (µL)	10

II.6.3 Production of lentiviral particles containing the CD63-GFP fusion construct by transfection of HEK-293FT cells

Transfection of HEK-293FT cells was performed by a second-generation lentiviral packaging system during five consecutive days. The protocol per day is described below.

Day 1. HEK-293FT cells were seeded in a 10 cm-culture plate (5 x 10^6 cells, 37°C, 5% CO_2) to end up with a plate confluency of around 70% after overnight incubation.

Day 2. The lentiviral (pLVX-CD63-GFP), packaging (psPAX2, Didier Trono Lab) and envelope (pMD2.G, Didier Trono Lab) plasmids were mixed in a polypropylene tube (4:3:1 for a total of 13 µg DNA) and 600 µL of OPTI-MEM medium (Thermo Fisher Scientific) was added to the plasmid mixture. Addition of the Transfection Reagent (Xfect, Takara Clontech, USA) directly into the OPTI-MEM/DNA mixture (0,3 µL Xfect per µg of DNA) was done previous to incubation at RT for 15 min. The transfection was performed by dropwise addition of the DNA/OPTI-MEN/Xfect mixture to HEK-293FT cells in culture medium (DMEM+10% FCS+P/S) and incubation for 12-15 hrs.

Day 3. Culture medium was replaced with a fresh one to remove the transfection reagent and cells were incubated for additional 24 hrs.

Day 4. Cell culture conditioned medium was harvested, transferred to a polypropylene tube and stored at 4°C. Fresh culture medium was added and cells were incubated for 24 hrs.

Day 5. Cell culture conditioned medium was harvested and pooled with the medium from the previous day. The pool of lentiviral particle-containing media was filtered (0.45 µm-filter, Sartorius Stedim, Biotech) to remove cells and stored at 4°C.

II.6.4 Transduction of HLF and SNU449 cells with lentiviral particles bearing the GFP-tagged CD63 construct

HLF and SNU449 cells were seeded in a 6-well culture plate (2 x 10^5 cells) and incubated overnight resulting in approximately 70% confluent wells. After plating, media were replaced with fresh culture media containing 8 µg/mL hexadimethrine bromide (Polybrene, Sigma-Aldrich). Lentiviral particle containing-medium was thawed up on ice and added to cells (1:5 of the cell culture medium). Cells were washed 24 hrs post-infection and fresh medium was added for additional 24 hrs. Selection with 2 µg/mL puromycin was carried out during 48 hrs prior to flow cytometry analysis of the transduced cells for detection of GFP.

II.7 Single cell cloning of CD63-GFP-expressing HLF and SNU449 cells

The pool of each CD63-GFP-expressing HLF and SNU449 cells were seeded in a 96-well plate for single cell cloning by limiting dilution (theoretically, an average of 1 cell per well). Cell culture media were changed twice a week and after three weeks, cells showing a single population were transferred to a 48-well plate. Cells were cultured and those showing expansion were transferred to larger culture plates until single cell clones (SCCs) were expanded into a 10 cm-culture plate. Twelve SCCs per cell line were tested for the expression of CD63-GFP fusion protein by immunoblotting and three of them showing the highest CD63 expression were selected for further experiments. The criterion for selection among the three SCCs was the production of the highest fraction of GFP-labeled EVs as compared with the pool of cells.

II.8 Immunofluorescence microscopy

HLF and SNU449 cells (parental and CD63-GFP transduced) were seeded in a 6-well tissue culture plate with a density of 5 x 10^5 and 10 x 10^5 cells, respectively. Previously, three cover slips were placed in each well and coated with collagen for at least 1 hr at RT followed by sucking off of the collagen excess. Cells were washed with pre-warmed PBS 24 hrs post-seeding followed by fixation with 4% formaldehyde for 15 min at 37°C. Washing three times with pre-warmed PBS for 2 min was carried out prior to staining with DAPI, 1:1000 (33342, Sigma-Aldrich) and phalloidin, 1:750 (R415, Invitrogen). For these nuclear and actin stainings, upside-down cover slips were incubated onto 30 µL of DAPI and palloidin in 1% BSA-PBS added on a parafilm (placed on the bottom of a 15 cm-culture plate used as a humidity chamber). After incubation for 1 hr in the dark, cover slips were washed three times with PBS every 5 min and embedded (upside-down) in a special anti-fade reagent dropped on

microscope slides (Prolong Gold Antifade Reagent, Molecular probes (Invitrogen), USA). Slides were dried during 2 days at 4°C and immunofluorescence microscopy with a 63x magnification in oil was performed to visualize cells expressing GFP (Confocal Laser Scanning Microscope, Zeiss, Germany).

II.9 Flow cytometry analysis of GFP-labeled cells and derived EVs

HLF and SNU449 cells transduced with the pLVX-CD63-GFP plasmid and selected with puromycin were analyzed by flow cytometry for detection of GFP (FACSCalibur, BD, USA). Both transduced HCC cell lines were positive for GFP and used for EV isolation.

EVs isolated from HLF and SNU449 cells (parental and CD63-GFP-transduced: pool of cells and SCCs) were analyzed by flow cytometry for detection of GFP (BD LSR Fortessa cell analyzer, Biosciences, USA; BD FACS Diva software, version 6.2). Parameters were adjusted for detection of EVs (Table 8) and flow cytometry data were analyzed with Flowing Software version 2.5.1. Flow cytometry standard operating procedures to detect EVs included a cleaning step for 1 hr prior to measurements. Read-outs of sterile-filtered ddH_2O and PBS (same volume that the corresponding EV sample) prior to each sample measurement were carried out in order to control the background. A cleaning step for 15 min among EV sample measurements was always the routine. For analysis of the data, events detected when measuring PBS (blank) were subtracted from those counted in the EV sample. In addition, a defined population of particles that was always present when measuring PBS and EV samples was considered as "noise" and excluded from the analysis. Gating of the GFP-positive population was carried out after measuring the negative controls. GFP percentage was calculated as the ratio between GFP-positive events and total events after background subtraction.

Table 8. Flow cytometer settings for detection of EVs

Parameter	***Voltage***	***Scale***
FSC	401	log
SSC	231	log
FITC	478	log
FSC threshold=1400		

II.10 Statistical analysis

Multiple comparison analyses were performed by one-way ANOVA and Tukey's test to determine the effect of EV treatment in HCC cells. Transcript levels of epithelial and mesenchymal markers of untreated and EV-treated HepG2 cells were compared independently of those of untreated HepG2, HLF and HLF-T cells. Comparison of the migration rates of HLF and HLF-T cells was performed by unpaired Student's t-test considering a two-tailed p-value. Significance levels were considered when $p<0.05$. All the analyses were performed using GraphPad Prism version 5.01.

III RESULTS

III.1 Characterization of EVs derived from HCC cells by NTA and immunodetection

EVs from cell culture conditioned medium (CCM) of HCC cell lines were isolated by DUC and using a membrane affinity-based kit. Use of these two approaches allowed selecting the best methodology for isolation of the vesicles, particularly by taking the enrichment of exosomes and quality of the EV samples into account. EVs were analyzed by NTA for estimation of the particle concentration and size. EV purification by DUC co-isolated a heterogeneous population of EVs. Size distribution plots of EV derived from HLF, HLF-T and SNU449 cells revealed a similar composition of EVs with different size ranges including exosomes (<150 nm in diameter) which represented 50-61% of the whole EV population (Figure 11A and 11B). In addition, EVs with a diameter between 150 and 200 nm and vesicles larger than 200 nm accounted for approximately 21-25% and 17-27 % of the total bioparticles, respectively. In contrast, EVs isolated by the membrane capture-based kit showed a lower representation of the exosome fraction accounting for 20%. The most prominent fraction in the kit-purified EVs was the one of the biggest particles (>200 nm in diameter) which reached more than 50% of the total vesicles.

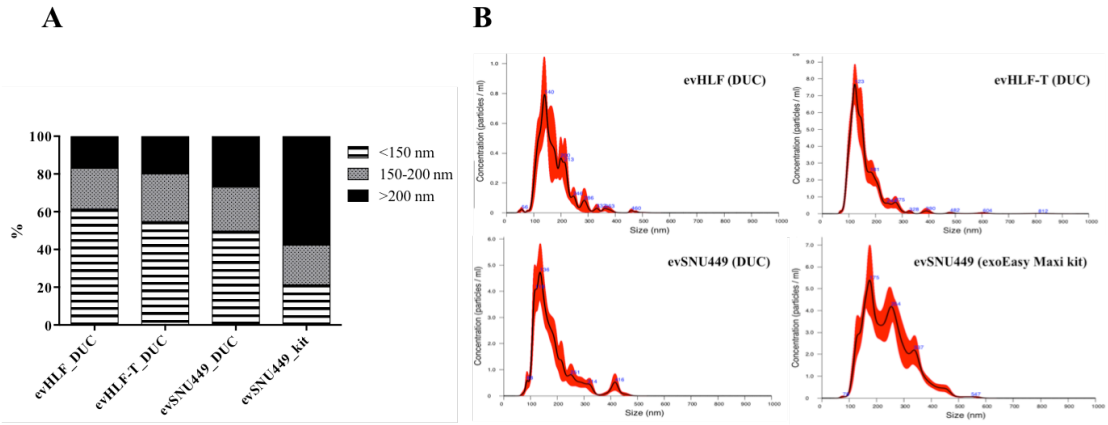

Figure 11. NTA characterization of HCC cell line-derived EVs isolated by DUC and exoEasy Maxi kit. A) Size distribution plots and B) NTA profiles of EVs derived from HLF, HLF-T and SNU449 cells.

Analysis of the EV isolation yield showed that SNU449 cells released a higher amount of vesicles as compared to HLF-T cells, and the latter cells produced more EVs than parental HLF cells (Figure 12). Furthermore, isolation of EVs using the membrane affinity-based kit yielded higher particles per volume of CCM in comparison to EVs isolated by DUC. Statistically significant differences were not found due to the high standard deviation of several EV isolations per cell line. This could be explained by the purification procedure *per se* since not all EV isolations were performed under the same technical conditions. For EV isolation by DUC, ultracentrifugation tubes were re-used which decreased the isolation yield with increasing ultracentrifugation cycles.

Characterization of EVs was further performed by immunodetection of EV markers which have been reported as one of the most specific for exosomes (Figure 13). HLF cell- and SNU449 cell-derived EVs showed a co-enrichment of the tetraspanin members CD63 and CD81 together with the unique presence of TSG101 as compared to their parental cells (Figure 13A). In contrast, the endoplasmatic reticulum protein GRP78 usually used as negative control for exosomes, was only detectable in cell lysates rather than in EVs. Actin was higher represented in cell lysates in comparison to EVs as expected for this housekeeping protein. Noteworthy, the tetraspanin members were much more abundant in SNU449 cell-derived EVs as compared to EVs isolated from HLF cells. In an attempt to detect at least one EV marker protein in kit-isolated EVs, vesicles derived from SNU449-CD63-GFP cells displayed a weaker signal of CD63 in comparison to EVs isolated by DUC (Figure 13B).

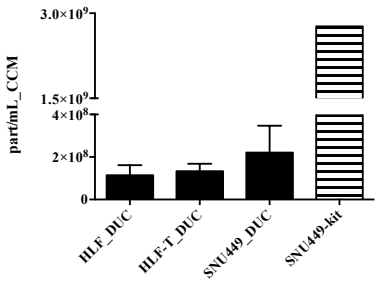

Figure 12. Yield of EVs in HCC cell lines after isolation by DUC (given by total particles per mL of CCM). SNU449-derived EVs were isolated by DUC and the exoEasy Maxi kit.

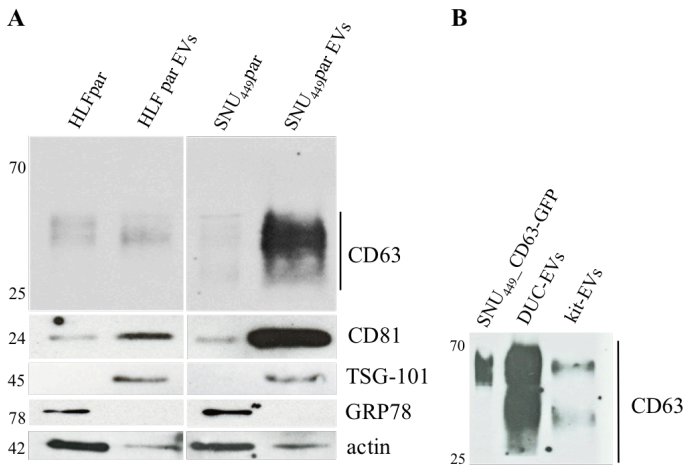

Figure 13. Detection of EV markers in cell and EV lysates by Western blotting. A) Western blot analysis of HFL and SNU449 cell and their derived EVs isolated by DUC. B) Western blot analysis of SNU449-CD63-GFP cells (left lane) and secreted EVs isolated by DUC (middle lane) and using the exoEasy Maxi kit (right lane).

Altogether these results showed that even though the yield of the EV isolation by DUC is lower as compared to that of the membrane affinity-based kit, there was a higher representation of CD63, CD81 and TSG101-harboring exosomes in the EV population purified by DUC. This explains the stronger immunodetection of CD63 in those DUC-isolated EVs in comparison to vesicles isolated by the membrane capture-based kit. Consequently, DUC was chosen as the EV isolation approach for further experiments despite a time-consuming protocol and the lower yield of total vesicles.

III.1.1 Stability and storage of EVs derived from HCC cells

In order to determine how stable EVs are at 4°C, the particle concentration and size of EV samples isolated either by DUC or using the membrane affinity-based kit were analyzed by NTA after storage for a maximum of 7 days (Figure 14A and 14B). DUC-isolated EVs showed a gradual decrease of the particle concentration when stored at 4°C as compared to the fresh sample (Figure 14A). Interestingly, EVs that were frozen at -80°C and thawed up prior to the NTA analysis displayed a particle concentration comparable to that of the fresh sample. Concerning the size, there were no remarkable changes in this parameter. However, EVs stored at 4°C for one day showed a reduction in the size that could be explained by the higher standard error of that measurement in comparison to the other ones. Likewise, the particle concentration of kit-isolated EVs decreased over the time when stored at 4°C as compared to samples that were frozen at -80°C and thawed up either quickly or slowly (Figure 14B). Notably, quick and slow thawing up of frozen EV samples refers to thawing up at 37°C and thawing up on ice, respectively. Storage at 4°C for more than a week revealed that after 12 days, the particle concentration was as low as the minimum that can be accurately measured by NTA (Figure 14C). The frozen sample at -80°C kept the highest particle concentration as seen in above-shown assays.

Since experiments using fresh EVs were difficult to plan due to the low yield of single EV isolations, frozen EV samples were pooled to increase the number of particles in most cases. In this respect, determination of the optimal conditions for freezing and thawing up of EVs was a critical point. Therefore, freezing at -20°C and -80°C as well as freeze/thaw cycles were tested (Figure 14D). The NTA measurements resulted in a higher particle concentration of EV samples frozen at -80°C as compared to those stored at -20°C. As positive control, a sample stored at 4°C for one day was used due to the impossibility of measuring the fresh EVs. In addition, two freeze/thaw cycles displayed a reduction in the number of particles of EVs frozen at -80°C. Therefore, these data suggest that freezing at -80°C with only one freeze/thaw cycle is the best condition for storing EV samples.

Finally, EVs frozen at -80°C and thawed up under two different conditions (quick at 37°C and slow at 4°C) were also measured by NTA (Figure 14E). This assay showed that -80°C-frozen EVs kept higher number of particles when the sample was quickly thawed up as compared to a slow thawing up. Thawed up EVs were stored at 4°C for 6 days and according to the results above-presented (Figure 14A), there was a decrease in the particle concentration over the time as compared to a sample stored at 4°C for one day after the EV isolation. In summary, the best condition for storage of EVs that cannot be used freshly for further assays is one cycle of

freezing at -80°C and quick thawing up at 37°C in order to keep the number of particles as high as possible.

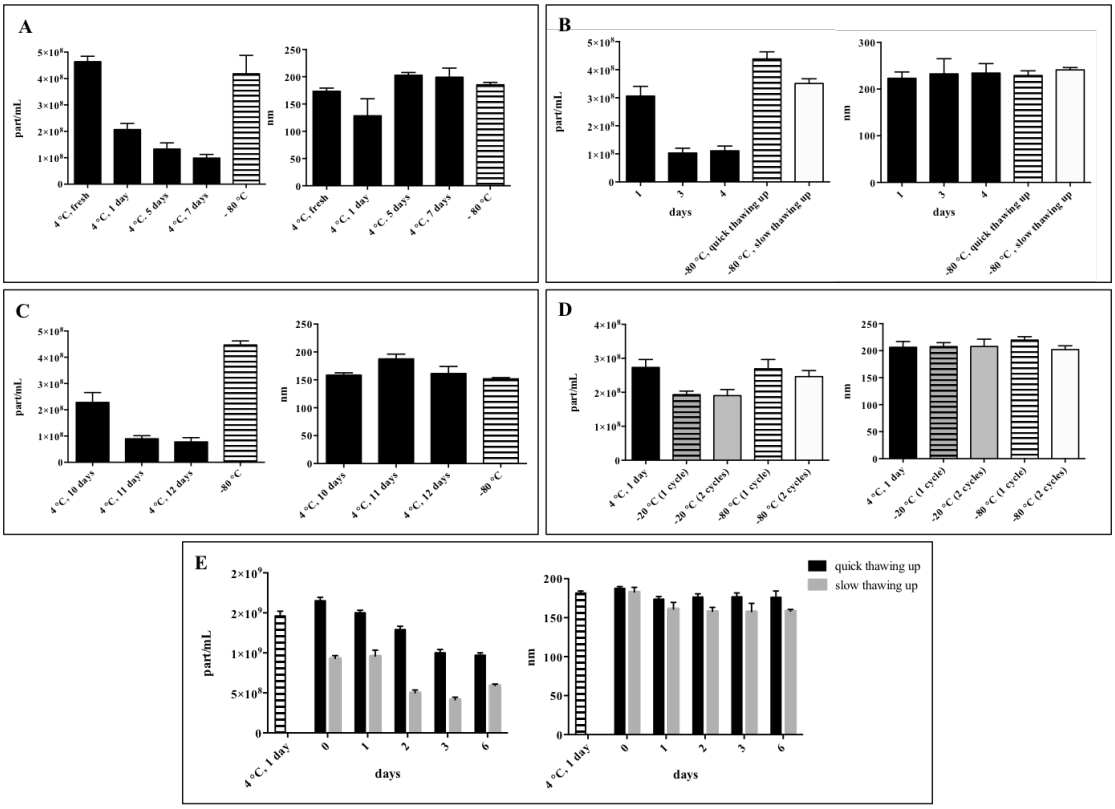

Figure 14. Stability of HCC cell-derived EVs stored at 4°C, -20°C and -80°C and thawed up quickly and slowly as measured by NTA. Particle concentration and size of EVs A) isolated by DUC and stored at 4°C up to 7 days, B) isolated by exoEasy Maxi kit and stored at 4°C up to 4 days, C) isolated by DUC and stored at 4°C up to 12 days, D) isolated by DUC and frozen at -20°C and -80°C with one and two freeze/thaw cycles and E) isolated by DUC and stored at 4°C up to 6 days after quick and slow thawing up from freezing at -80°C. Bars represent mean ± standard error of single measurements with six image captures.

III.2 Epithelial HepG2 cells show a change in cell plasticity upon treatment with EMT-transformed HCC cell-derived EVs

To study whether EVs isolated from EMT-transformed HCC cells might have an impact on the cell plasticity of epithelial HCC cells, HepG2 cells were treated with HLF cell- and HLF-T cell-derived EVs. HLF-T cells refer to HLF cells treated with TGF-β1 for more than 10 days. This long-term TGF-β1-treatment is not able to induce EMT in epithelial human HCC cells (e.g. HepG2 cells) in contrast to the effect of this cytokine on malignant transformed mouse hepatocytes with an epithelial phenotype[43,44]. However, TGF-β1 treatment of mesenchymal human HCC cells (i.e., HLF cells) endows these cells (named HLF-T cells) with a higher migration rate as revealed by scratch assays (Figure 15). In addition, HLF-T cells show the ability to form tumors after xenotransplantation into immunodeficient SCID mice while parental HLF cells fail to generate tumors (Haider C. et. al., 2018, manuscript in preparation).

Single EV treatment of HepG2 cells was performed for 24 and 72 hrs. Noteworthy, the experiment was carried out with exponentially growing cells (Figure S1). EVs derived from HLF-T cells were characterized by immunoblotting confirming the enrichment of CD63, lack of the endoplasmatic reticulum protein GRP78 and lower detection of actin as compared to cell lysates (Figure 16).

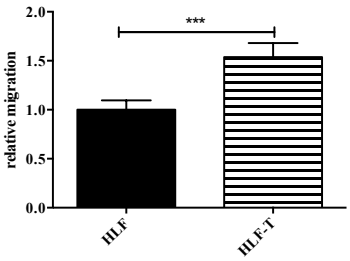

*Figure 15. Relative migration of HLF-T cells as compared to parental HLF cells. Bars represent mean ± SD of two independent scratch assays. Unpaired Student's t test was performed. *** p<0.001*

EV-treated HepG2 cells displayed lower CDH1 (E-cadherin) mRNA levels as compared to untreated HepG2 cells (Figure 17A). However, this difference was significant only between untreated cells and HepG2 cells treated with EVs derived from HLF-T cells for 72 hrs (Figure 17A, right panel). It is expected that the statistical analyses of both treatments do not show the same results since the treatment for 72 hrs was performed in three independent experiments whereas the treatment for 24 hrs was carried out as a unique experiment with two replicates. This might explain why the significant difference between the negative control and HepG2 cells treated with HLF-T cell-derived EVs for 72 hrs but not after treatment for 24 hrs. Furthermore, in both time point treatments there was a significant difference between EMT-transformed HLF and HLF-T cells and untreated epithelial HepG2 cells. This was expected considering that E-cadherin is an epithelial marker which is downregulated in mesenchymal-like cells.

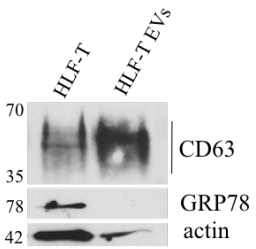

Figure 16. Detection of CD63, GRP78 and actin in HLF-T cell-derived EVs by Western blotting.

According to the epithelial and mesenchymal states displayed by HepG2 cells and HLF/HLF-T cells, respectively, mRNA levels of mesenchymal markers were higher in the latter cells (Figure 17B-17G). Interestingly, transcript levels of Snail2 in HLF cells were at the same level of those in HepG2 cells (Figure 17C) suggesting that not all the EMT-TFs are upregulated in mesenchymal-like cells. However, HLF-T cells showed a higher expression of Snail2 in comparison with HLF cells suggesting that the long-term TGF-β1 treatment is responsible for the positive regulation of this EMT-TF. Noteworthy, expression levels of another EMT-TF (Zeb2) were analyzed but those were too low for accurate detection in both HepG2 and HLF/HLF-T cells (data not shown). The statistical significance between the mRNA levels of the mesenchymal markers in HepG2 and HLF/HLF-T cells varied between the two time point treatments. This might be explained by the different experimental settings of both treatments as well as the standard deviation of the measurements, which were unexpectedly higher for some of the mesenchymal markers.

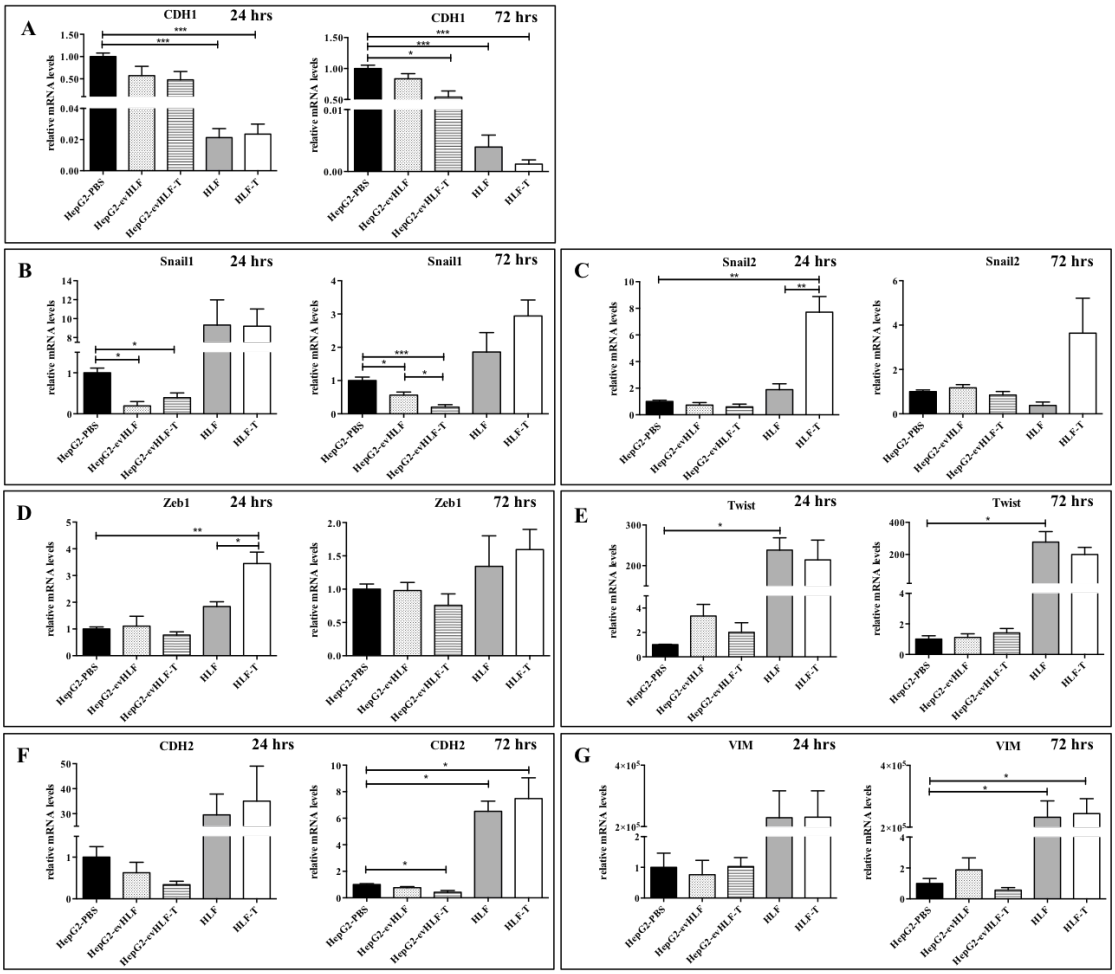

*Figure 17. Normalized transcript levels of epithelial and mesenchymal markers in HepG2 cells treated with HCC cell-derived EVs as well as HLF and HLF-T cells for 24 hrs (left) and 72 hrs (right) as compared to untreated HepG2 cells. Relative mRNA levels of A) CDH1, B) Snail1, C) Snail2, D) Zeb1, E) Twist, F) CDH2 and G) VIM. Bars represent mean ± SEM. Statistical analysis was performed by ANOVA and Tukey's test. * $p<0.05$, ** $p<0.01$, *** $p<0.001$*

Mesenchymal markers including EMT-TFs such as Snail1, Snail2, Zeb1 and Twist as well as N-cadherin (CDH2) and vimentin were not upregulated upon EV treatment (Figure 17B-17G). It was expected that at least some EMT-TFs which are transcriptional repressors of CDH1 show higher expression levels according to the decreased mRNA levels of this epithelial marker after EV treatment. Interestingly, Snail1 and N-cadherin displayed even a significant downregulation of their mRNA levels in EV-treated HepG2 cells (Figure 17B and 17F).

In summary, EV treatment of HepG2 cells showed that EVs derived from EMT-transformed HCC cells induced changes in the cell plasticity of these epithelial HCC cells by downregulation of E-cadherin. Reduction of E-cadherin expression levels was stronger upon stimulus with HLF-T cell-derived EVs for 72 hrs. Furthermore, E-cadherin downregulation was independent of the transcriptional repression exerted by EMT-TFs and upregulation of

other mesenchymal markers such as N-cadherin and vimentin. Contradictory, Snail1 and N-cadherin displayed a reduction of their gene expression levels in EV-treated HepG2 cells.

III.3 CD63-GFP-transduced HLF and SNU449 cells secrete GFP-labeled EVs

Tools for *in vivo* EV education of mice prior to xenografting of HCC cells were generated by transduction of HLF and SNU449 cells with a plasmid bearing a CD63-GFP fusion construct. CD63-GFP-expressing HCC cell lines were expected to secrete GFP-labeled EVs which can be injected into immunodeficient mice for detection of EV-recipient cells in putative target organs.

After cloning of the lentiviral plasmid bearing the CD63-GFP fusion gene in *E. coli* and prior to transfection of the purified plasmid DNA into HEK-293FT cells, a restriction enzyme analysis was carried out in order to confirm the identity of the fusion construct (Figure 18). As expected, digestion of the plasmid (about 8.9 kbp) with the double-cutting restriction enzyme BspHI resulted in DNA fragments of 7892 and 1008 bp. After digestion with PmlI, two DNA fragments of approximately 5616 and 3285 bp were generated. In summary, the analysis of the purified plasmid DNA with restriction enzymes showed that the lentiviral plasmid harbors the expected CD63-GFP fusion gene.

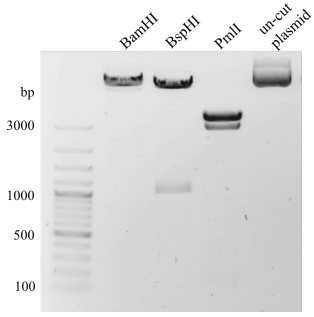

Figure 18. Restriction enzyme analysis of the lentiviral plasmid harboring the CD63-GFP fusion gene.

CD63-GFP-transduced HLF and SNU449 cells were selected with puromycin and analyzed by flow cytometry in order to confirm the expression of the plasmid. Both HCC cell lines were positive for GFP signal (Figure 19). EVs derived from CD63-GFP-transduced HCC cell lines were characterized by immunoblotting using the same panel of EV markers specific for exosomes (Figure 20A). According to above-shown immunoblottings, the tetraspanin members CD63 and CD81 were co-enriched in EVs and TSG101 was only present in the bioparticles when compared to cell lysates. EVs were negative for GRP78 detection and actin was higher abundant in cells than in vesicles. Furthermore, the immunoblotting showed that EVs derived from parental and transduced SNU449 cells harbor more CD63 as compared to parental and transduced HLF cell-derived EVs. CD63-GFP-transduced cells and derived EVs showed a signal at higher molecular weight when detecting CD63 which revealed the expression and presence of the fusion protein. Parental cells and derived EVs were devoid of

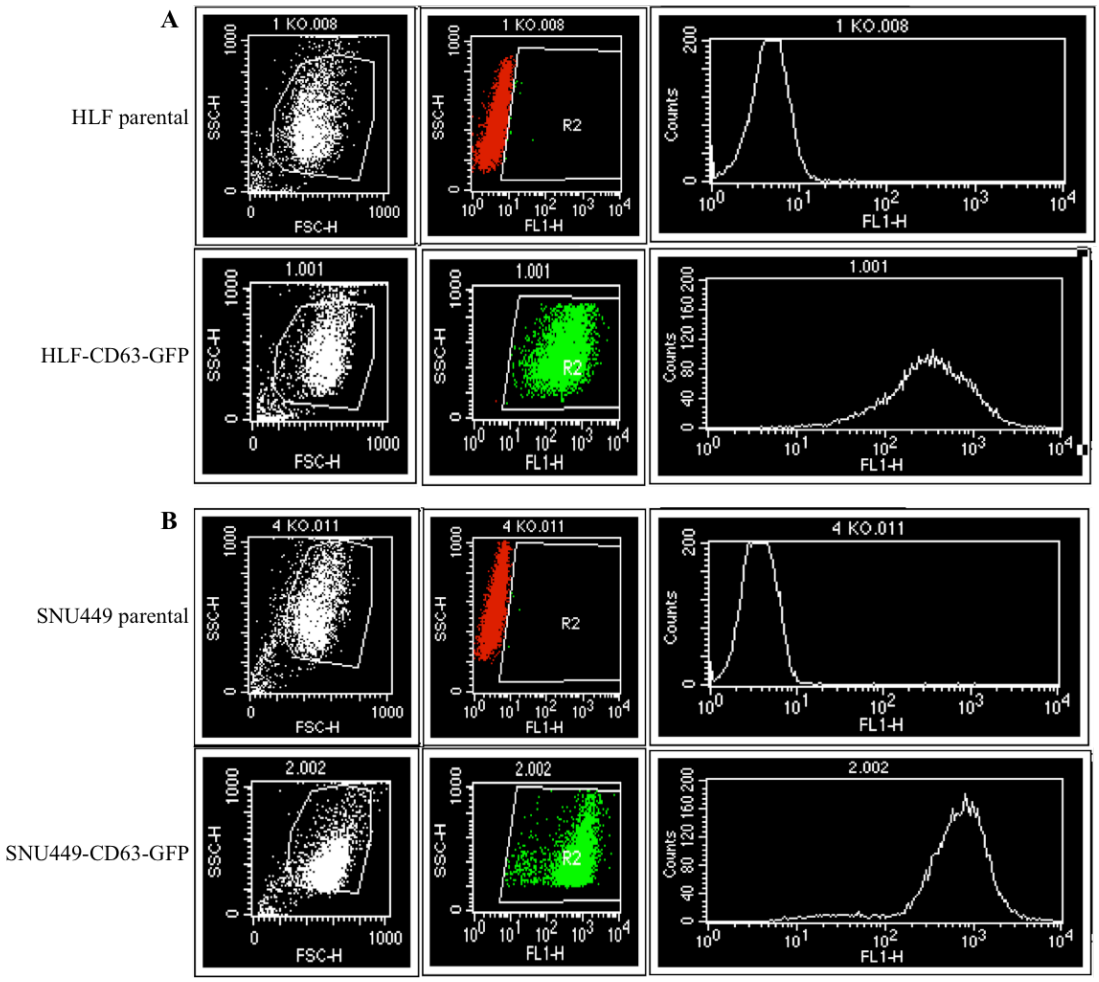

Figure 19. Scatter plots and histograms of parental and CD63-GFP-transduced HCC cells as detected by flow cytometry. A) HLF parental (upper panel) and transduced cells (lower panel). B) SNU449 parental (upper panel) and transduced cells (lower panel).

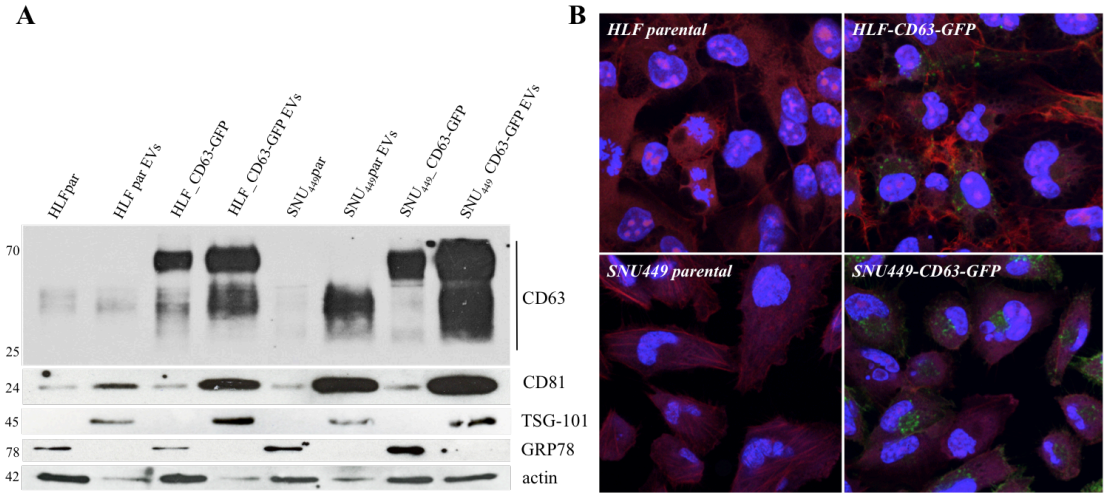

Figure 20. Detection of EV markers and CD63-GFP fusion protein in transduced cells and derived EVs. A) Detection of EV markers in cell and EV lysates by Western blot analysis. Immunoblotting of parental and CD63-GFP-transduced HFL (left panel) and SNU449 cells (right panel) and their derived EVs isolated by DUC. B) Immunofluorescence microscopy of parental and CD63-GFP-transduced HLF and SNU449 cells for detection of GFP (63x magnification in oil).

the CD63-GFP fusion protein (Figure 20A). GFP expression was detected by immunofluorescence microscopy in cells transduced with the fusion construct as compared to parental cells (Figure 20B). The immunofluorescence analysis revealed a stronger GFP expression in transduced SNU449 cells in comparison to transduced HLF cells. This suggested that SNU449-CD63-GFP cells express higher levels of the fusion protein. This result matches with the detection levels of CD63 in EVs isolated from these two transduced HCC cell lines (Figure 20A).

To further confirm the GFP labeling of the bioparticles, flow cytometry analysis of EVs derived from CD63-GFP-transduced cells was performed. Prior to these measurements, selection of the appropriate dilutions of the EV samples was carried out as a pre-requisite for reliable flow cytometry analyses. A dilution curve was measured with EV samples derived from these two HCC cell lines (Figure 21 and Figure S2). Importantly, there was a positive and linear correlation between particle concentration and number of events. The results suggested that signals detected by the cytometer were generated from individual particles indicating that the tested EV concentrations could be used for further measurements. Notably, the parallel increase in the total number of events with and without blank subtraction (background events in PBS) indicated that the background was kept at the same level among all the measurements.

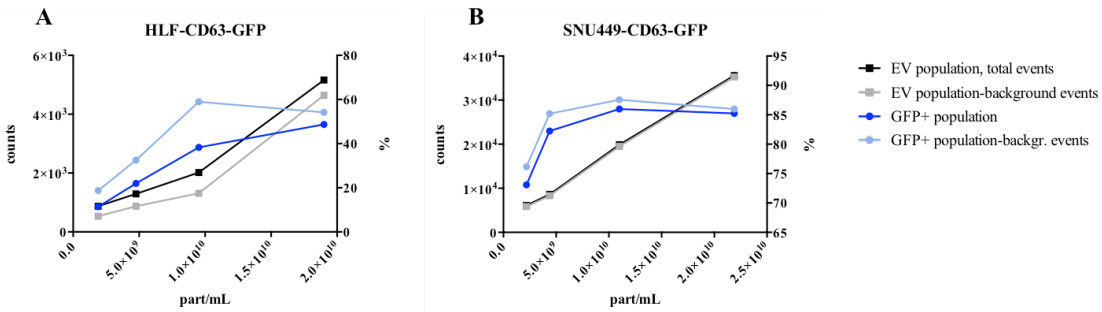

Figure 21. Dilution curve of EVs derived from CD63-GFP-expressing A) HLF and B) SNU449 cells as analyzed by flow cytometry. Background events refer to those present in PBS which were subtracted (-background events) or not subtracted from the EV population events (total events) detected in EV samples. Left and right axes represent counts (number of events) and percentage of the GFP-positive EV population, respectively.

The percentage of GFP-positive population with increasing EV concentrations showed a plateau at a particle concentration of 1 x 10^{10} particles/mL in the case of HLF cell-derived EVs (Figure 21A). This plateau was reached at a lower concentration of SNU449 cell-derived EVs (5 x 10^{9} particles/mL) (Figure 21B), as expected since those cells released a higher number of GFP-labeled particles. Noteworthy, the plateau in the percentage of GFP-positive population with the gradual increase of the EV concentration was expected. Remarkably, there was an increase of GFP percentage with increasing EV concentrations at particle

concentrations lower than the above-mentioned values. This trend might indicate that the background affects the GFP percentage at those low particle concentrations. Even though PBS was measured as blank and taken into account in the mathematical analysis, the dilution in PBS *per se* entails a higher background in more diluted EV samples in comparison to more concentrated ones. This intrinsic background due to the dilution of the EV samples in PBS decreased the calculated percentage of GFP-labeled EVs. From these data we concluded that the flow cytometry analyses of EVs must be performed at a particle concentration higher than 1 x 10^{10} particles/mL to avoid the influence of the background. After determining the appropriate range of particle concentrations to be used for flow cytometry measurements of EVs, vesicles derived from CD63-GFP-expressing HLF and SNU449 cells were detected (Figure 22).

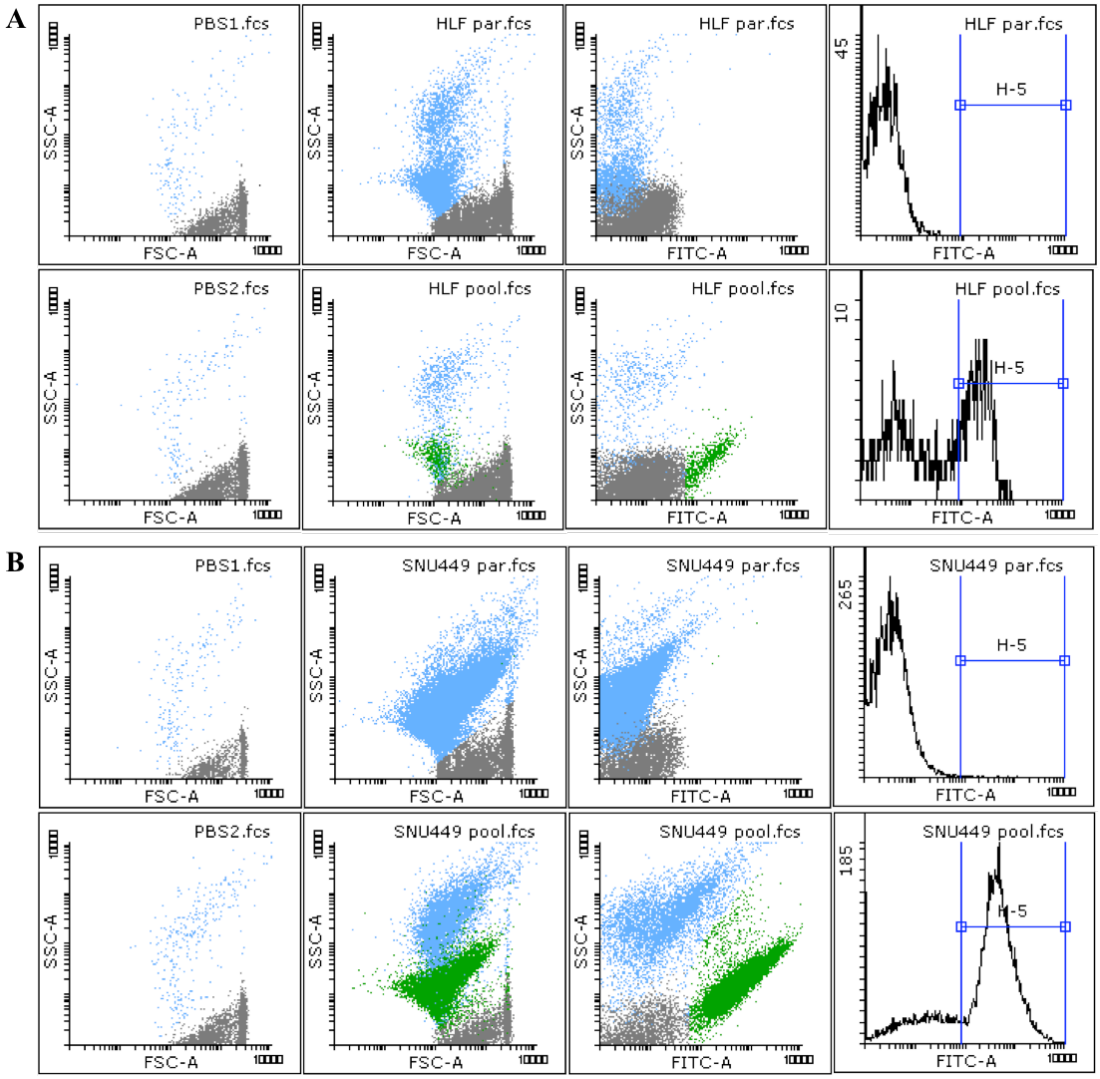

Figure 22. Scatter plots and histograms of EVs derived from A) HLF and B) SNU449 parental and CD63-GFP-transduced cells as detected by flow cytometry. Upper and lower panels in A) and B) represent EVs derived from parental and transduced cells, respectively. The concentration of EV samples was 1.3 x 10^{10} particles/mL as quantified by NTA. Gray, blue and green events represent noise, EV population and GFP-positive EV population, respectively.

The amount of GFP-positive particles was indicated by the height of the peak whereas the fluorescence intensity was given by the right shift in the FITC channel of the histograms (Figure 22). Scatter plots and histograms confirmed the above-shown findings that SNU449 cells release a larger GFP-labeled population of EVs with a higher intensity (Figure 22B, lower panel) in comparison to HLF cells (Figure 22A, lower panel). In summary, these results corroborated what was indicated by the immunoblotting for detection of CD63 and the immunofluorescence analysis for detection of GFP only in cells. EVs derived from transduced SNU449 cells contain a larger population of GFP-positive particles resulting in a higher fluorescence intensity due to their elevated CD63 enrichment as compared to HLF cell-derived EVs (Figure 13A) as well as the increased exogenous expression of the CD63-GFP protein in transduced SNU449 cells (Figure 20).

Since the pools of CD63-GFP-expressing SNU449 and HLF cells released different amounts of GFP-labeled EV population, single cell clones (SCCs) were generated from each cell line. Three out of twelve SCCs per cell line were further analyzed in order to select the one producing the highest amount of GFP-labeled EVs with the highest intensity. Immunoblotting as well as immunofluorescence analyses showed that the SCCs expressed the CD63-GFP fusion protein (Figure 23). However, Western blotting and immunofluorescence analyses showed little differences when detecting CD63 and GFP signals, respectively, among the SCCs and the pool of cells. Immunofluorescence microscopy showed that in the case of GFP-labeled-HLF cells (Figure 23A), SCC8 seemed to have a higher GFP expression as compared to the pool of cells and other SCCs. Likewise, SCC8 slightly exceeded CD63 expression as compared to the pool of transduced HLF cells and other SCCs as revealed by Western blot analysis (Figure 23A). In the case of GFP-expressing-SNU449 cells, SCC1 exhibited the strongest signal for CD63 as shown by the Western blot analysis of the cell lysates (Figure 23B). However, the pool of cells and the SCCs showed comparable levels of GFP expression by immunofluorescence microscopy (Figure 23B). To further compare the SCCs with the pool of cells, flow cytometry analysis of EVs isolated from these cells was performed.

Flow cytometry detection of the pool of GFP-labeled EVs as well as SCC-derived EVs showed that a SCC per cell line could be chosen as the one releasing the most intense and the highest percentage of GFP-labeled EVs (Figure 24). With regard to HLF-SCCs (Figure 24A), SCC8 (68.7%) and SCC10 (69.9%) displayed the highest percentage of GFP-positive EV population as compared to EVs derived from the pool of HLF cells (61.1%). However, HLF-SCC10 cells were discarded due to the differences of SCC10-derived EVs observed in the scatter plot and histogram. Notably, SCC8-derived EVs displayed a higher fraction of GFP-positive EVs with higher fluorescence intensity as compared to vesicles derived from the pool

of HLF cells. This result corresponded to the strongest CD63 and GFP signals of SCC8 shown by Western blotting and immunofluorescence microscopy (Figure 23A).

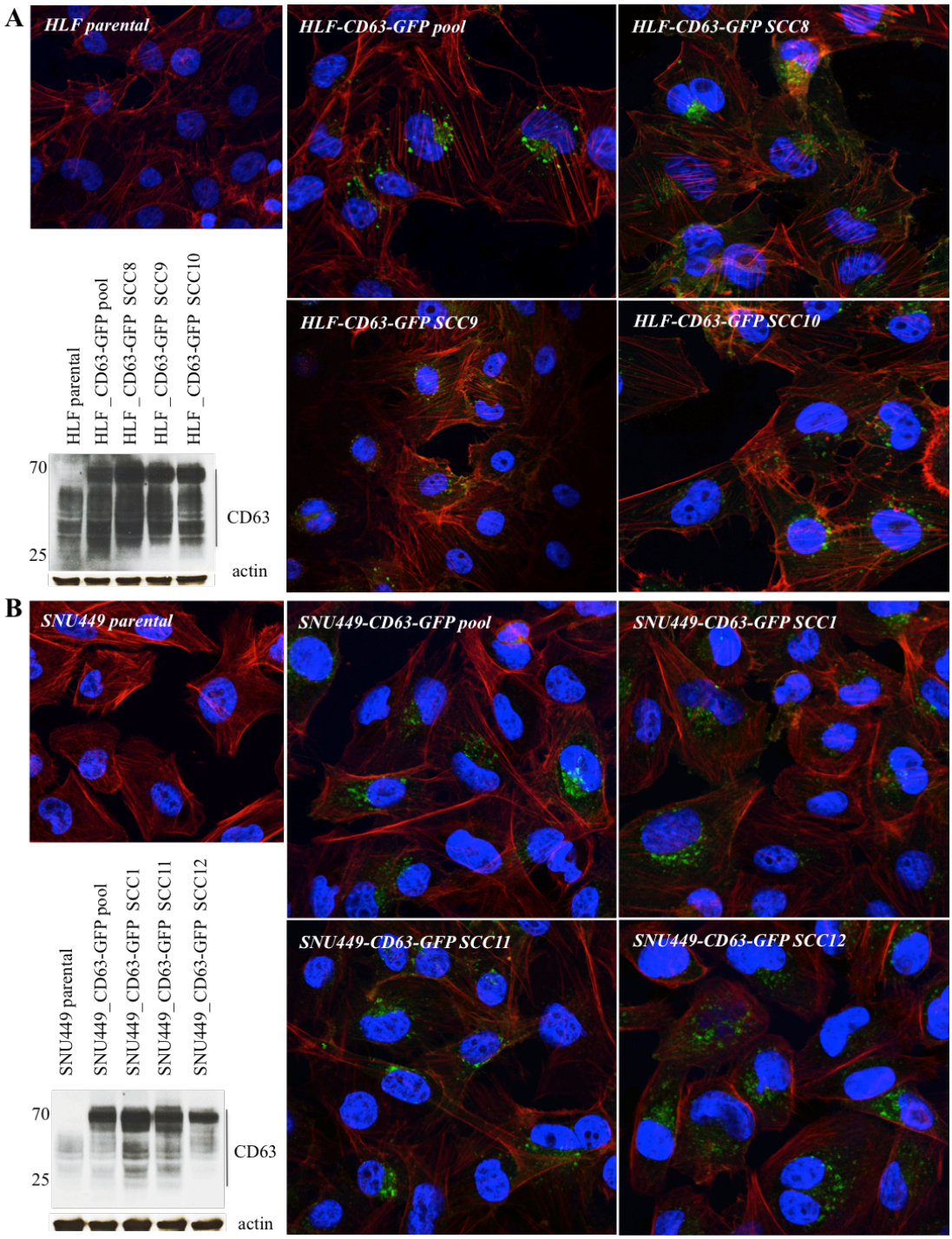

Figure 23. Detection of CD63-GFP fusion protein in parental and CD63-GFP-expressing pools of A) HLF B) and SNU449 cells and their corresponding SCCs by Western blot analysis of cell lysates and immunofluorescence microscopy (63x magnification in oil).

Among the EVs derived from GFP-expressing SNU449 cells (Figure 24B), SCC1 showed the highest percentage of GFP-positive EV population (99.6%) with the strongest fluorescence signal among the SCCs. In addition, SCC1 exhibited a higher fraction of GFP-labeled EVs as

compared to the pool of cells (72.4%). However, SCC1 displayed a comparable number of GFP-labeled EVs with similar fluorescence intensity as compared to EVs derived from the pool of SNU449 cells. As shown by scatter plots and histograms of these two EV samples, the pool of CD63-GFP-transduced cells was enriched with high levels of a GFP-negative EV population that reduced the percentage of GFP-positive EVs to 72.4%. The nature of the EV population devoid of GFP signal is unknown so far and might include microvesicles as well as apoptotic bodies which were not present in EVs isolated from SCC1. Noteworthy, the flow cytometry analysis of SCC1 confirmed the results shown by Western blotting (Figure 23B).

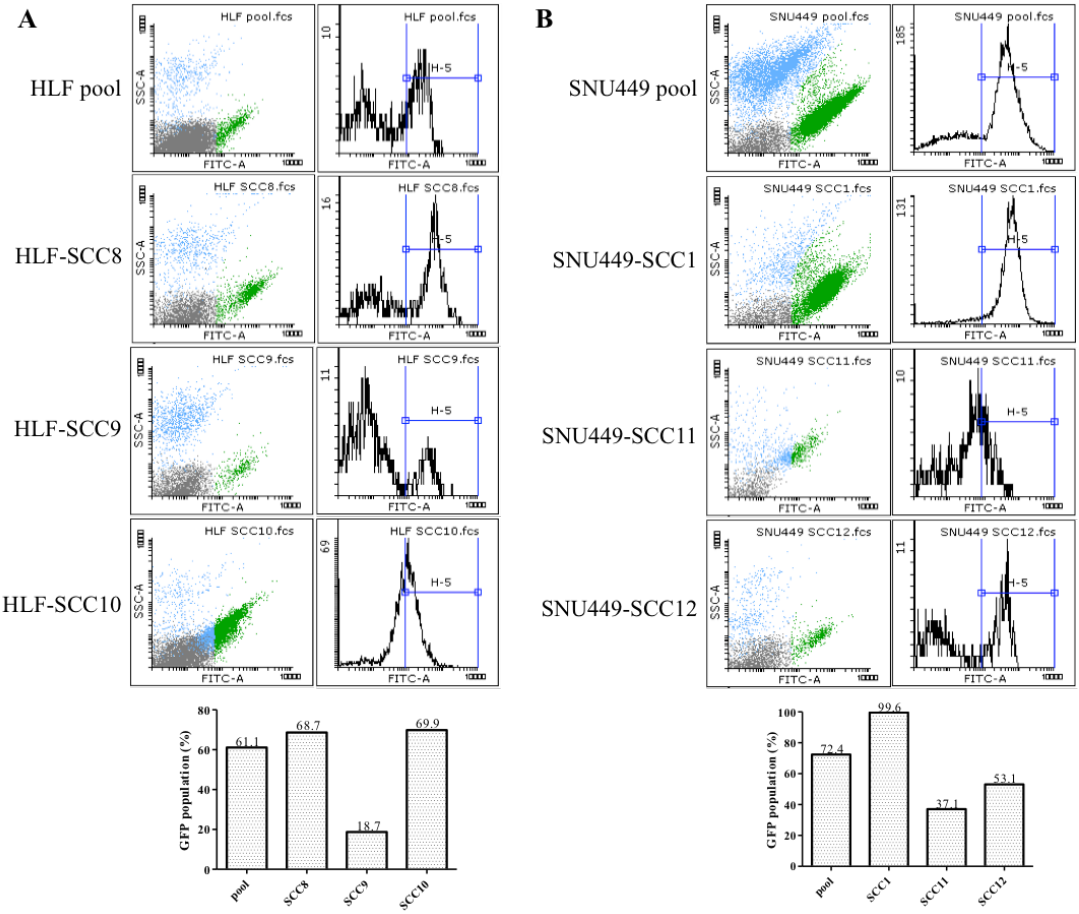

Figure 24. Scatter plots and histograms of EVs derived from CD63-GFP-expressing pools of A) HLF and B) SNU449 cells and their corresponding SCCs as detected by flow cytometry. Gray, blue and green events represent noise, EV population and GFP-positive EV population, respectively. The lower panel includes graphs representing the GFP-labeled EV population (%) of the pool of cells and SCCs.

Even though the selection of SCCs resulted in subclones releasing a higher fraction of GFP-labeled EVs for both cell lines, HLF-SCC8 showed a lower representation of GFP-positive population (68.7%) as compared to SNU449-SCC1 (99.6%). This was expected since EVs derived from SNU449 cells displayed an increased enrichment of CD63 in comparison to HLF cell-derived EVs. Noteworthy, despite the lower GFP percentage, the fluorescence intensity of GFP-labeled EVs derived from HLF-SCC8 was comparable to that of SNU449-SCC1. This highlights the positive outcome of having performed single cell cloning of the

pools of transduced HCC cells. In summary, HCC cells expressing CD63-GFP such as HLF-SCC8 as well as SNU449-SCC1 will be used for *in vivo* education of mice with GFP-labeled EVs.

IV DISCUSSION

In this study, single particle sizing and quantification of EVs were performed by NTA which is commonly used for characterization of EVs due to the ease of sample preparation for measurements and fast read-outs. Even though electron microscopy has been described as the gold standard approach to evaluate the quality of EV samples as well as the vesicle size, the current study did not benefit from this technique. Noteworthy, NTA analysis shows several limitations based on the operating principle *per se* as well as variations in the reproducibility[45]. For that reason, quantification of the protein concentration of EV samples was performed in parallel with NTA estimation of the particle concentration when EVs were used for *in vitro* treatment of HepG2 cells. These double measurements based on different entities, proteins and particles allowed us to have a more reliable values to reproduce the EV treatment with the same protein/cell and particle/cell ratios in biological replicates.

The EV treatments of HepG2 cells were performed with approximately 0.3 ng of EV proteins per cell (0.3 ng/cell). This EV protein/cell ratio is comparable to those reported in publications demonstrating the role of sEVs in promoting motility, invasiveness and stemness of recipient cells. For instance, a study reporting the induced migration and invasion of non-motile immortalized human hepatocytes upon treatment with sEVs derived from highly metastatic HCC cells for 48 hrs used a ratio of 0.1-0.2 ng/cell[30]. Another publication reporting the induction of EMT in urothelial cells treated with sEVs derived from muscle-invasive human bladder cancer cells performed the EV treatment with 0.3 ng/cell for 24 hrs[31]. EVs derived from human prostate cancer cells upon hypoxia used at a ratio of 0.1 ng/cell were shown to promote invasiveness as well as stemness of the same cancer cells under normoxia[32]. In summary, the number of EVs used for treatment of recipient cells in the current study was expected to produce appreciable effects in HepG2 cells.

EV isolation by DUC and the exoEasy Maxi kit demonstrated that the former is the most suitable approach for co-isolation of a mixed population of EVs with the highest fraction of exosomes. The representation of exosomes among the EVs derived from all the cell lines used in this study was either equal to or higher than 50% when isolated by DUC (Figure 11A). This resulted in the expected immunodetection of a panel of positive EV markers such as CD63, CD81 and TSG-101 which have been described as the most specific for exosomes (Figure 13A). Assuming that particles larger than 150 nm are plasma membrane-derived

vesicles and apoptotic bodies, it is interesting that EV samples were negative for GRP78 as the larger particles represented approximately 50% of the whole EV population. This apparent contradiction might be explained by two factors. Firstly, the lower protein amount from those larger vesicles as compared to cell lysates was insufficient for GRP78 detection. Secondly, due to the impossibility of measuring the fresh samples, the size distribution plots corresponded to EV samples with a -80°C-freeze/37°C-thaw cycle prior to NTA measurements (Figure 11A). It is possible that those stored EV samples showed slight differences based on the formation of exosome clumps or aggregations as compared to fresh EVs. This would explain higher sizes when measuring thawed EV samples by NTA which not necessarily reflect the presence of larger vesicles such as plasma membrane-derived vesicles and apoptotic bodies. In summary, it is probable that the exosome fraction in the EV samples was underestimated. Consequently, GRP78 was not detected even in the presence of larger vesicles which were likely overestimated. Thus, our results highlight that the repertory of positive and negative EV markers used in this study for specific detection of exosomes does not rule out the presence of other vesicles which might constitute up to 50% of the total EV population.

In case that fresh EVs cannot be used for further experiments, freezing of EVs at -80°C and quick thawing up at 37°C demonstrated to be the optimal storage condition for preserving the highest number of particles (Figure 14D and 14E). Importantly, preservation of the biological activity of EVs after a single -80°C-freeze/37°C-thaw cycle was observed in the *in vitro* treatment of HepG2 cells performed with EV samples stored under that condition.

It is unclear why SNU449 cells released the highest amount of EVs since those cells as well as HLF cells show a very comparable cellular phenotype in culture and are not able to generate tumors in immunodeficient mouse models after xenotransplantation. However, the slightly higher EV yield of HLF-T as compared to HLF cells (Figure 12) can be explained by phenotypical changes as HLF-T cells exhibit a higher migratory behavior (Figure 15) and the ability to form tumors after xenografting (Haider C. et. al., 2018, manuscript in preparation). These two characteristics indicate the increased malignancy of HLF-T cells when compared to HLF cells. In accordance with the literature, malignant progression and the increase in the metastatic potential of tumor cells correlate with EV release[24]. In this regard, a study reported that among HCC cell lines with different motile abilities and non-motile immortalized human hepatocytes, HCC cell lines released a higher number of sEVs which correlated with an increased amount of protein content in comparison to the healthy hepatocytes. Furthermore, among the HCC cell lines, the highly malignant ones with an enhanced motility released sEVs harboring higher amount of tumorigenic RNAs and proteins. sEVs derived from those

malignant HCC cell lines induced healthy hepatocytes to migrate and invade upon treatment[30]. Altogether, the biological cargo of EVs and their effects in recipient cells as well as the amount of released bioparticles is dictated by the malignancy of primary cancer cells.

Another difference between the EVs derived from the HCC cell lines used in this study was based on the abundance of membrane-associated proteins. As shown by immunodetection, EVs derived from SNU449 cells were enriched in the tetraspanin members CD63 and CD81 in comparison to HLF cell-derived EVs (Figure 13A). This result was not dependent on a higher representation of exosomes in EVs derived from SNU449 cells since all the tested HCC cell lines showed a comparable exosome fraction (Figure 11A). In this line, it is an open issue whether SNU449 cells harbor a distinct cargo in their EVs as compared to HLF cell-derived EVs. This distinct feature of SNU449 cell-derived EVs was advantageous in order to obtain GFP-labeled EVs by the fluorescent labeling system based on genetic engineering carried out in this study.

The downregulation of E-cadherin in HepG2 cells upon EV stimulus for 72 hrs demonstrated to be stronger with EVs derived from HLF-T cells in comparison to HLF cells (Figure 17A). This suggests two possible scenarios which can be independent or interconnected. Firstly, stimulus with HLF-T cell-derived EVs needs more than 24 hrs to have a significant effect on the expression level of this epithelial marker. However, due to the different experimental settings of both time point treatments, this conclusion remains unclear. Secondly, the observed phenomenon might reflect the tumor-promoting role of TGF-β. This cytokine could perform its effect not only directly on cells as shown with HLF cells but it is conceivable that TGF-β also modulates the cargo of secreted EVs. EVs derived from HLF-T cells might have a distinct cargo as compared to bioparticles derived from HLF cells owing to their more potent effect on the transcriptional downregulation of E-cadherin after 72 hrs.

To rule out the possibility of protein aggregates present in the EV pellet which might have some effect in the recipient cells, EV uptake by HepG2 cells could be assayed using GFP-labeled EVs. Consequently, GFP might have been detected in HepG2 cells by immunofluorescence microscopy. This would have allowed us to confirm that the observed effects in HepG2 cells upon EV treatment were caused by either biomolecules bound to the EV membrane or contained in their cargo.

In order to explain the downregulation of E-cadherin, the lack of the concomitant upregulation of EMT-TFs as well as other key mesenchymal markers such as N-cadherin and vimentin and the decrease in the mRNA levels of Snail1 and N-cadherin (Figure 17), a mechanistic molecular model has been proposed. We hypothesize that Snail1 protein could be

delivered via EVs into HepG2 cells to transcriptionally target E-cadherin. By a negative feedback loop, Snail1 represses the transcription of the endogenous Snail1 gene without affecting other EMT inducers for a period of 72 hrs. In fact, it has been reported that Snail1 negatively controls its own transcription by binding to either its promoter or the promoter of its transcriptional activator, resulting in a robust negative feedback loop which tightly controls Snail1 expression[46]. Noteworthy, this model assumes that the transcription factor Snail1 is exported to the cytoplasm and sorted into the EV cargo despite the short half-life of the protein which is between 20 and 45 min[46]. Once in the EV cargo, Snail1 should be delivered into recipient cells in a transcriptionally active form able to exert its repressive functions. However, the downregulation of N-cadherin is still elusive in this model and needs further experiments to be unraveled.

In a further attempt to explain the independent mRNA reduction of E-cadherin in the current study, epigenetic modification could represent an alternative mechanism. For instance, hypermethylation of CpG islands in the CDH1 promoter region by DNA methyltransferase I (DNMTI) causes epigenetic silencing of this epithelial marker in HCC cells[47]. A study in human breast cancer revealed that hypermethylation of the E-cadherin promoter rather than inactivating mutations of E-cadherin is associated with the EMT program. In this study, fibroblastic breast tumor cell lines with methylated E-cadherin promoter showed upregulation of Snail2 but not Snail1 and Twist[48]. Interestingly, epigenetic regulation of EMT-TFs is also a common event including DNA methylation, histone modifications and modulation by a complex network of RNAs interference. In fact, all these epigenetic modifiers can be found to collaborate with each other in order to induce or repress a mesenchymal-like phenotype. A conceivable, direct and negative regulation of E-cadherin by EV-delivered miRNAs or long non-coding RNAs has not been published so far to our knowledge[49].

Altogether the above-mentioned data might suggest that an epigenetic modifier delivered by EVs could be responsible of the observed downregulation of E-cadherin in our study. However, those epigenetic factors do not act on their own and need the cooperation of EMT-TFs which provide them with the required specificity to target CDH1[49]. In this regard, EMT-TFs can directly target E-cadherin and together with nuclear protein complexes involved in epigenetic control modulate the reprograming and cellular differentiation processes occurring during EMT[49]. Therefore, the most explanatory model is the one involving the transfer of Snail1 from mesenchymal to epithelial HCC cells via EVs to directly target E-cadherin. In fact, EVs have been reported to harbor nuclear transcription factors upon kidney injury[50] as well as in nasopharyngeal carcinoma[51]. Indeed, transfer of the biologically active form of an oncogenic transcription factor, hypoxia-inducible factor-1α (HIF-1α) via EVs enhanced

migration and invasion of nasopharyngeal cells. Those cells displayed a reduction and an increase of E-cadherin and N-cadherin protein levels, respectively, suggesting the induction of the EMT program upon EV stimulus[51]. Noteworthy, our data do not indicate the delivery of TGF-β by EVs since this cytokine induces EMT through transcriptional upregulation of EMT-TFs, a phenomenon which was not observed in our experiments.

Furthermore, non-upregulation of mesenchymal markers upon EV treatment (Figure 17B-17E) could also be a result of inducing a partial state between the epithelial and mesenchymal phenotypes. This would explain the reduction in the expression levels of the epithelial marker while there was not gain of mesenchymal traits. What still remains elusive is whether a partial induction of the EMT program in HepG2 cells might be associated with an enhanced malignancy based on the differentiation state of these cells.

Previous findings from our laboratory revealed that malignant HRas-transformed mouse hepatocytes with different genetic backgrounds are induced to a complete EMT program by TGF-β. This mechanism was responsible for an increased invasive behavior *in vitro* and malignancy *in vivo* of those EMT-transformed mouse hepatocytes[43,44]. The mesenchymal-like phenotype displayed by those hepatocytes was characterized by a depolarized and spindle-shaped morphology and accompanied by molecular changes such as loss of E-cadherin and β-catenin at the cell borders and nuclear translocation of SMAD2. Interestingly, induction of the EMT program was linked to nuclear accumulation of β-catenin which endowed HRas-transformed hepatocytes with stem cancer cell-like characteristics[52]. In that study, nuclear accumulation of β-catenin was activated by TGF-β-induced PDGF and led to tumor growth arrest and anchorage independent cell growth. This suggested that EMT-transformed hepatocytes exhibit more potent invasive abilities but also a less differentiated and dormant phenotype which could contribute to HCC chemoresistance and recurrence after surgical resection. In fact, a more recent publication confirmed that nuclear accumulation of β-catenin in Ras-transformed hepatocytes treated with TGF-β led to orthotopic liver tumors in mice composed of immature progenitor hepatocytes displaying either cytoplasmic redistribution or loss of E-cadherin[53]. Those findings were consistent with poorly differentiated human HCC tumors showing a lower representation of the membrane-bound fraction of E-cadherin in parallel with an increased nuclear β-catenin stabilization. These features correlated with the recurrence rate after orthotopic liver transplantation in human HCC patients[53]. In our study, it would be interesting to investigate whether the induction of an intermediate EMT state in HepG2 cells upon EV treatment is linked to higher levels of nuclear β-catenin leading to a less differentiated and malignant cell phenotype.

Generation of HCC cells secreting GFP-labeled EVs by transduction of a lentiviral plasmid bearing the fusion construct CD63-GFP was successful and shows an advantage with respect to other fluorescent-labeling approaches. In contrast to other methodologies that make use of either staining with fluorescent membrane dyes which are not specific for exosomes or antibody based-fluorescent labeling, our methodology based on the stable exogenous expression of a CD63-GFP fusion gene yields labeled EVs. In this regard, the fluorescent labeling step with membrane dyes or antibodies entails additional washing and ultracentrifugation steps which decrease the recovery and quality of EVs. Due to the high speed needed for pelleting the sEVs, some particles might be not recovered and others can undergo membrane rupture[41].

Dilution curves of EVs derived from CD63-GFP-transduced HLF and SNU449 cells demonstrated that the detection of the vesicles by flow cytometry was free from the swarm effect (Figure 21). The swarm effect refers to the drop in the number of events and overestimation of the size and fluorescence with increasing concentrations of the sample. This is caused because highly concentrated EV samples produce coincidence events. This term means that the cytometer is not able to discriminate between more than a particle that overlap in time and localize at the same measuring spot[54]. This results in an increased and unique signal from multiple and independent events that have been detected simultaneously as a single one by the cytometer. In this study, increasing concentrations of the EV samples resulted in higher number of events confirming a reliable flow cytometry analysis that is free of coincidence events with the tested ranges of particle concentrations. In this respect, 1.3 x 10^{10} particles/mL was chosen as the working particle concentration to detect GFP-labeled EVs since the expected plateau in the percentage of GFP-positive population was reached between 1.0 x 10^{10} and 2.19 particles/mL.

Another critical factor during flow cytometry analysis of EVs is a calibration step with submicron sized-beads to determine the resolution of the device for detection of the smallest vesicles. This preliminary step would be important in order to assess the minimal particle size that the cytometer is able to detect. In addition, establishment of a correspondence between forward and side light scatterings and EV sizes would be helpful for interpretation of the data. However, further analysis could benefit by setting the threshold based on the fluorescence intensity rather than the forward light scattering. That would make the detection independent of the size resolution of the cytometer. Future detection of fluorescence-labeled EVs should take into account these aspects with the aim of improving flow cytometry analysis of bioparticles.

The combined analysis of SCCs generated from the pools of CD63-GFP-transduced HLF and SNU449 cells revealed that the selection was successful (Figure 23 and 24). A SCC per cell line showed to release a more enriched fraction of GFP-labeled EVs as compared to EVs derived from the pool of cells. However, due to the distinct features of EVs derived from these two HCC cell lines, HLF-SCC8-derived EVs could not reach the same GFP percentage as EVs derived from SNU449-SCC1. This preliminary information will be critical when performing future *in vivo* experiments in which detection of GFP by immunohistochemistry will be performed.

IV.1 Concluding remarks and future perspectives

This project highlights the biological activity of EVs for horizontal transfer of still unknown biomolecules leading to changes in the epithelial plasticity of HCC cells. Downregulation of the epithelial marker E-cadherin which has been considered an invasion and metastasis suppressor was not accompanied with the classical gain of mesenchymal markers, but rather downregulation of Snail1 and N-cadherin. We postulated a mechanistic model in order to explain this apparent contradiction: export of Snail1 from HLF and HLF-T cells via EVs could directly target endogenous CDH1 gene and collaterally target the Snail1 gene in HepG2 cells. This scenario agrees with the induction of an intermediate epithelial-mesenchymal state in HepG2 cells upon EV stimulus.

Pursuing the phenomena leading to changes in the epithelial cell plasticity might benefit from changes in the conditions of the EV treatment in future experiments. Design of EV treatments with a higher dose of EVs, repeated EV stimuli rather than a single one over the treatment period or a treatment longer than 72 hrs are alternatives to be tested. All these possibilities could be assayed either independently or in combination in order to analyze whether there is a stronger downregulation of E-cadherin. Likewise, EMT-TFs and other mesenchymal markers should also be included in the analysis with the aim of monitoring a stronger induction of the EMT program. Additionally, migration of EV treated-HepG2 cells could be evaluated by wound healing assay.

Quantification of the protein expression levels of these markers upon EV stimulus would be helpful to corroborate the above-mentioned model. Whether Snail1 is delivered to HepG2 cells via EVs, protein and mRNA levels of Snail1 might not be correlated. This study has assumed that modulation of the epithelial plasticity of HepG2 cells is driven by the transcriptional regulation of E-cadherin. However, effectors delivered via EVs might orchestrate a transient regulation of E-cadherin by modulation of its protein levels. Reduction of E-cadherin protein levels leading to disruption of the adherens junctions is driven by different mechanisms that also account for modulation of the epithelial plasticity. For

instance, loss of E-cadherin function could be mediated by extracellular proteolytic cleavage[55], phosphorylation by tyrosine-kinases, ubiquitination and subsequent proteosomal degradation[18] or clathrin-mediated endocytosis for lysosomal degradation[10]. Quantification of the cytoplasmic and membrane-associated pools of E-cadherin would bring new insight about the regulation mechanisms induced by EV treatment. Furthermore, quantification of the membrane-bound fraction of β-catenin as well as its nuclear levels could be assessed in order to link induction of a partial or full EMT program to a putative more malignant dedifferentiated phenotype in HepG2 cells.

To test whether EVs can serve for horizontal and bidirectional transfer of information between these HCC cells, EVs derived from HepG2 cells might be used for treatment of HLF and HLF-T cells. Analysis of the mRNA and protein expression levels of the same panel of epithelial and mesenchymal markers would allow evaluating whether there is an induction of a MET program or changes in the mesenchymal plasticity of HLF and HLF-T cells.

RNA sequencing and proteomic profiling of the cargo of EVs derived from HLF and HLF-T cells are promising tools to elucidate the mechanisms leading to downregulation of E-cadherin. The analysis of transcripts and proteins in EVs that are differentially released by these two cells could highlight the involvement of TGF-β in promoting changes in the epithelial plasticity by modulating the specific cargo of the secreted vesicles. Even though the cargo of those EVs present a comparable composition, the relative abundance of some RNAs and/or proteins could simultaneously give an insight of the effector leading to downregulation of CDH1 and the differences between HLF/HLF-T cell-derived EVs.

The current investigation made some progress in characterization and storage of EVs derived from HCC cell lines following a DUC-based EV isolation approach. Despite the time-consuming protocol and the low yield of total particles from those cell lines, EV populations contained a representative fraction of exosomes as verified by NTA and immunodetection. Therefore, DUC was the method of choice for EV isolation. Even though EV isolation by a membrane capture-based kit yielded a lower fraction of exosomes, a future project might take advantage of this commercial product due to its fast and easy protocol. EVs recovered by the kit could be used either in an additional ultracentrifugation step to pellet sEVs or an ultrafiltration step to exclude the larger vesicles. In summary, combination of the membrane affinity-based kit with other approaches should be tested and optimized to increase the exosome fraction in those EV samples, thus saving time and efforts simultaneously.

This study established the best condition for storage of EVs derived from two HCC cell lines extensively used in our laboratory. This opened the possibility of planning experiments with

EVs at any time when storing these biological vesicles at -80°C. After a thawing up step at 37°C, EVs retain a number of particles comparable to that of fresh samples and demonstrated to exert a biological activity in cell communication.

Immunodetection demonstrated to be a suitable technique for characterization of EVs derived from different cells. In this regard, we reported that HCC cell-derived EVs present different levels of tetraspanin members such as CD63 and CD81, being SNU449 cell-derived EVs the ones with the highest enrichment. This had implications in the production of CD63-GFP-labeled EVs for future *in vivo* experiments. In this regard, generation of GFP-tagged CD63-expressing HCC cell lines by stable transduction of a plasmid bearing the fusion gene demonstrated to be a suitable approach for the production of GFP-labeled EVs without need of further processing. GFP-labeled EVs were easily analyzed by a combination of techniques, each providing different as well as redundant information and making the interpretation of data more reliable.

Advances in flow cytometry analysis of EVs have also been made. Determination of the appropriate concentration range for a reliable detection of the vesicles and calculation of the GFP-positive EV fraction was the preliminary assay. Adjustment of the flow cytometer parameters have been proposed in order to improve the detection of fluorescent labeled-EVs by setting a threshold based on the fluorescence intensity. Since flow cytometry detection of fluorescent-labeled EVs is a faster and easier technique to detect those vesicles as compared to immunoblotting, the procedure should be optimized.

A future research project will analyze whether EVs are involved in pre-metastatic niche formation in HCC making use of the GFP-labeled EVs. This hypothesis will be tested by the injection of fluorescent-labeled EVs into immunodeficient mouse models. Administration routes of the EVs as well as the time window after injection and prior to tissue collection have to be determined. Mouse tissue collection from probable target organs will be followed by immunohistochemistry for detection of GFP to reveal whether EVs were uptaken by cells. Detection of cell type-specific markers in those cells will bring information of the EV recipient cells in those organs. In the case that EV uptake is successful, xenotransplantation of HCC cell lines with non-tumor formation abilities is expected to produce tumor outgrowth in the EV-educated mice. Even though xenografted mice with HLF and SNU449 cells do not develop tumors, injection of EVs derived from e.g. HLF-T cells will serve to evaluate whether there is a change in the microenvironment of putative target organs. Detection of increased fibronectin secretion as an event of ECM deposition and quantification of factors involved in stromal microenvironment remodeling such as MMPs will allow understanding the processes activated by EV uptake in those organs. Xenotransplantation of HepG2 cells in

educated mice with EVs derived from HLF-T cells could be a more feasible alternative to investigate the role of EVs in forming a pre-metastatic niche in the liver. Considering that HepG2 cells exhibit tumor formation abilities, EV education of mice would allow us to monitor an enhancement in tumor growth and likely an increased metastatic outgrowth[56]. In summary, molecular and cellular changes associated with EV uptake in mouse models will highlight the impact of EVs as mediators of long range signaling on HCC progression.

REFERENCES

1. McGlynn, K. A., Petrick, J. L. & London, W. T. Global epidemiology of hepatocellular carcinoma: an emphasis on demographic and regional variability. *Clin. Liver Dis.* **19,** 223–238 (2015).

2. Ramakrishna, G. *et al.* From Cirrhosis to Hepatocellular Carcinoma: New Molecular Insights on Inflammation and Cellular Senescence. *Liver Cancer* **2,** 367–383 (2013).

3. Marquardt, J. U., Andersen, J. B. & Thorgeirsson, S. S. Functional and genetic deconstruction of the cellular origin in liver cancer. *Nat. Rev. Cancer* **15,** 653 (2015).

4. Golabi, P. *et al.* Mortality assessment of patients with hepatocellular carcinoma according to underlying disease and treatment modalities. *Medicine (Baltimore)* **96,** (2017).

5. He, M. *et al.* Hepatocellular carcinoma-derived exosomes promote motility of immortalized hepatocyte through transfer of oncogenic proteins and RNAs. *Carcinogenesis* **36,** 1008–1018 (2015).

6. Giannelli, G., Koudelkova, P., Dituri, F. & Mikulits, W. Role of epithelial to mesenchymal transition in hepatocellular carcinoma. *J. Hepatol.* **65,** 798–808 (2016).

7. Giannelli, G. *et al.* The rationale for targeting TGF-β in chronic liver diseases. *Eur. J. Clin. Invest.* **46,** 349–361 (2016).

8. Bataller, R. & Brenner, D. A. Liver fibrosis. *J. Clin. Invest.* **115,** 209–218 (2005).

9. Zucman-Rossi, J., Villanueva, A., Nault, J.-C. & Llovet, J. M. Genetic Landscape and Biomarkers of Hepatocellular Carcinoma. *Gastroenterology* **149,** 1226–1239.e4 (2015).

10. Thiery, J. P., Acloque, H., Huang, R. Y. J. & Nieto, M. A. Epithelial-Mesenchymal Transitions in Development and Disease. *Cell* **139,** 871–890 (2009).

11. Nieto, M. A., Huang, R. Y.-J., Jackson, R. A. & Thiery, J. P. EMT: 2016. *Cell* **166,** 21–45 (2016).

12. Hirohashi, S. & Kanai, Y. Cell adhesion system and human cancer morphogenesis. *Cancer Sci.* **94,** 575–581 (2003).

13. van Zijl, F., Krupitza, G. & Mikulits, W. Initial steps of metastasis: Cell invasion and endothelial transmigration. *Mutat. Res. Mutat. Res.* **728,** 23–34 (2011).

14. Moon, H. *et al.* Transforming Growth Factor-β Promotes Liver Tumorigenesis in Mice via Up-regulation of Snail. *Gastroenterology* **153,** 1378–1391.e6 (2017).

15. Grusch, M. *et al.* The Crosstalk of RAS with the TGF-β Family During Carcinoma Progression and its Implications for Targeted Cancer Therapy. *Curr. Cancer Drug Targets* **10,** 849–857 (2010).

16. Li, H.-Y. *et al.* Activation of TGF-β1-CD147 positive feedback loop in hepatic stellate cells promotes liver fibrosis. *Sci. Rep.* **5,** (2015).

17. Yang, M. *et al.* A double-negative feedback loop between Wnt–β-catenin signaling and HNF4α regulates epithelial–mesenchymal transition in hepatocellular carcinoma. *J Cell Sci* **126,** 5692–5703 (2013).

18. Yang, J. & Weinberg, R. A. Epithelial-Mesenchymal Transition: At the Crossroads of Development and Tumor Metastasis. *Dev. Cell* **14,** 818–829 (2008).

19. Affo, S., Yu, L.-X. & Schwabe, R. F. The Role of Cancer-Associated Fibroblasts and Fibrosis in Liver Cancer. *Annu. Rev. Pathol.* **12,** 153–186 (2017).

20. Sanz-Cameno, P., Trapero-Marugán, M., Chaparro, M., Jones, E. A. & Moreno-Otero, R. Angiogenesis: From Chronic Liver Inflammation to Hepatocellular Carcinoma. *Journal of Oncology* (2010). doi:10.1155/2010/272170

21. Au, S. H. *et al.* Clusters of circulating tumor cells traverse capillary-sized vessels. *Proc. Natl. Acad. Sci.* **113,** 4947–4952 (2016).

22. Stoletov, K. *et al.* Visualizing extravasation dynamics of metastatic tumor cells. *J Cell Sci* **123,** 2332–2341 (2010).

23. Kanada, M., Zhang, J., Yan, L., Sakurai, T. & Terakawa, S. Endothelial cell-initiated extravasation of cancer cells visualized in zebrafish. *PeerJ* **2,** (2014).

24. Peinado, H., Lavotshkin, S. & Lyden, D. The secreted factors responsible for pre-metastatic niche formation: old sayings and new thoughts. *Semin. Cancer Biol.* **21,** 139–146 (2011).

25. Soung, Y. H., Ford, S., Zhang, V. & Chung, J. Exosomes in Cancer Diagnostics. *Cancers* **9,** (2017).

26. Kowal, J. *et al.* Proteomic comparison defines novel markers to characterize heterogeneous populations of extracellular vesicle subtypes. *Proc. Natl. Acad. Sci. U. S. A.* **113,** E968-977 (2016).

27. Théry, C., Zitvogel, L. & Amigorena, S. Exosomes: composition, biogenesis and function. *Nat. Rev. Immunol.* **2,** 569 (2002).

28. Johnstone, R. M., Adam, M., Hammond, J. R., Orr, L. & Turbide, C. Vesicle formation during reticulocyte maturation. Association of plasma membrane activities with released vesicles (exosomes). *J. Biol. Chem.* **262,** 9412–9420 (1987).

29. Syn, N., Wang, L., Sethi, G., Thiery, J.-P. & Goh, B.-C. Exosome-Mediated Metastasis: From Epithelial-Mesenchymal Transition to Escape from Immunosurveillance. *Trends Pharmacol. Sci.* **37,** 606–617 (2016).

30. He, M. *et al.* Hepatocellular carcinoma-derived exosomes promote motility of immortalized hepatocyte through transfer of oncogenic proteins and RNAs. *Carcinogenesis* **36,** 1008–1018 (2015).

31. Franzen, C. A. *et al.* Urothelial cells undergo epithelial-to-mesenchymal transition after exposure to muscle invasive bladder cancer exosomes. *Oncogenesis* **4,** e163 (2015).

32. Ramteke, A. *et al.* Exosomes secreted under hypoxia enhance invasiveness and stemness of prostate cancer cells by targeting adherens junction molecules. *Mol. Carcinog.* **54,** 554–565 (2015).

33. Chowdhury, R. *et al.* Cancer exosomes trigger mesenchymal stem cell differentiation into pro-angiogenic and pro-invasive myofibroblasts. *Oncotarget* **6,** 715–731 (2015).

34. Webber, J. P. *et al.* Differentiation of tumour-promoting stromal myofibroblasts by cancer exosomes. *Oncogene* **34,** 290 (2015).

35. Hoshino, A. *et al.* Tumour exosome integrins determine organotropic metastasis. *Nature* **527,** 329 (2015).

36. Costa-Silva, B. *et al.* Pancreatic cancer exosomes initiate pre-metastatic niche formation in the liver. *Nat. Cell Biol.* **17,** 816 (2015).

37. Yu, Z. *et al.* Pancreatic cancer-derived exosomes promote tumor metastasis and liver pre-metastatic niche formation. *Oncotarget* **8,** 63461–63483 (2017).

38. Kamerkar, S. *et al.* Exosomes facilitate therapeutic targeting of oncogenic KRAS in pancreatic cancer. *Nature* **546,** 498 (2017).

39. Garcia-Contreras, M., Brooks, R., Boccuzzi, L., D.Robbins, P. & Ricordi, C. Exosomes as biomarkers and therapeutic tools for type 1 diabetes mellitus. *Eur. Rev. Med. Pharmacol. Sci.* **21,** 2940–2956 (2017).

40. Willms, E. *et al.* Cells release subpopulations of exosomes with distinct molecular and biological properties. *Sci. Rep.* **6,** 22519 (2016).

41. Lobb, R. J. *et al.* Optimized exosome isolation protocol for cell culture supernatant and human plasma. *J. Extracell. Vesicles* **4,** (2015).

42. Melo, S. A. *et al.* Glypican-1 identifies cancer exosomes and detects early pancreatic cancer. *Nature* **523,** 177 (2015).

43. Gotzmann, J. *et al.* Hepatocytes convert to a fibroblastoid phenotype through the cooperation of TGF-beta1 and Ha-Ras: steps towards invasiveness. *J. Cell Sci.* **115,** 1189–1202 (2002).

44. Fischer, A. N. M. *et al.* Integration of Ras subeffector signaling in TGF-β mediated late stage hepatocarcinogenesis. *Carcinogenesis* **26,** 931–942 (2005).

45. Vestad, B. *et al.* Size and concentration analyses of extracellular vesicles by nanoparticle tracking analysis: a variation study. *J. Extracell. Vesicles* **6,** (2017).

46. De Herreros, A. G., Peiró, S., Nassour, M. & Savagner, P. Snail family regulation and epithelial mesenchymal transitions in breast cancer progression. *J. Mammary Gland Biol. Neoplasia* **15,** 135–147 (2010).

47. QIU, X., QIAO, F., SU, X., ZHAO, Z. & FAN, H. Epigenetic activation of E-cadherin is a candidate therapeutic target in human hepatocellular carcinoma. *Exp. Ther. Med.* **1,** 519–523 (2010).

48. Lombaerts, M. *et al.* E-cadherin transcriptional downregulation by promoter methylation but not mutation is related to epithelial-to-mesenchymal transition in breast cancer cell lines. *Br. J. Cancer* **94,** 661–671 (2006).

49. Skrypek, N., Goossens, S., Smedt, E. D., Vandamme, N. & Berx, G. Epithelial-to-Mesenchymal Transition: Epigenetic Reprogramming Driving Cellular Plasticity. *Trends Genet.* **33,** 943–959 (2017).

50. Zhou, H. *et al.* Urinary exosomal transcription factors, a new class of biomarkers for renal disease. *Kidney Int.* **74,** 613–621 (2008).

51. Aga, M. *et al.* Exosomal HIF1α supports invasive potential of nasopharyngeal carcinoma-associated LMP1-positive exosomes. *Oncogene* **33,** 4613–4622 (2014).

52. Fischer, A. N. M. *et al.* PDGF essentially links TGF-beta signaling to nuclear beta-catenin accumulation in hepatocellular carcinoma progression. *Oncogene* **26,** 3395–3405 (2007).

53. Zulehner, G. *et al.* Nuclear β-Catenin Induces an Early Liver Progenitor Phenotype in Hepatocellular Carcinoma and Promotes Tumor Recurrence. *Am. J. Pathol.* **176,** 472–481 (2010).

54. Kormelink, T. G. *et al.* Prerequisites for the analysis and sorting of extracellular vesicle subpopulations by high-resolution flow cytometry. *Cytometry A* **89,** 135–147 (2016).

55. Heuberger, J. & Birchmeier, W. Interplay of Cadherin-Mediated Cell Adhesion and Canonical Wnt Signaling. *Cold Spring Harb. Perspect. Biol.* **2,** (2010).

56. Govaere, O. *et al.* The PDGFRα-laminin B1-keratin 19 cascade drives tumor progression at the invasive front of human hepatocellular carcinoma. *Oncogene* **36,** 6605–6616 (2017).

SUPPLEMENTARY MATERIAL

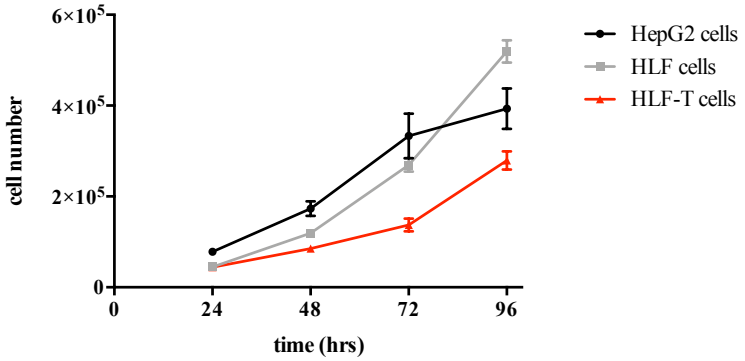

Figure S1. Growth curves of HepG2, HLF and HLF-T cells during the EV treatment for 72 hrs.

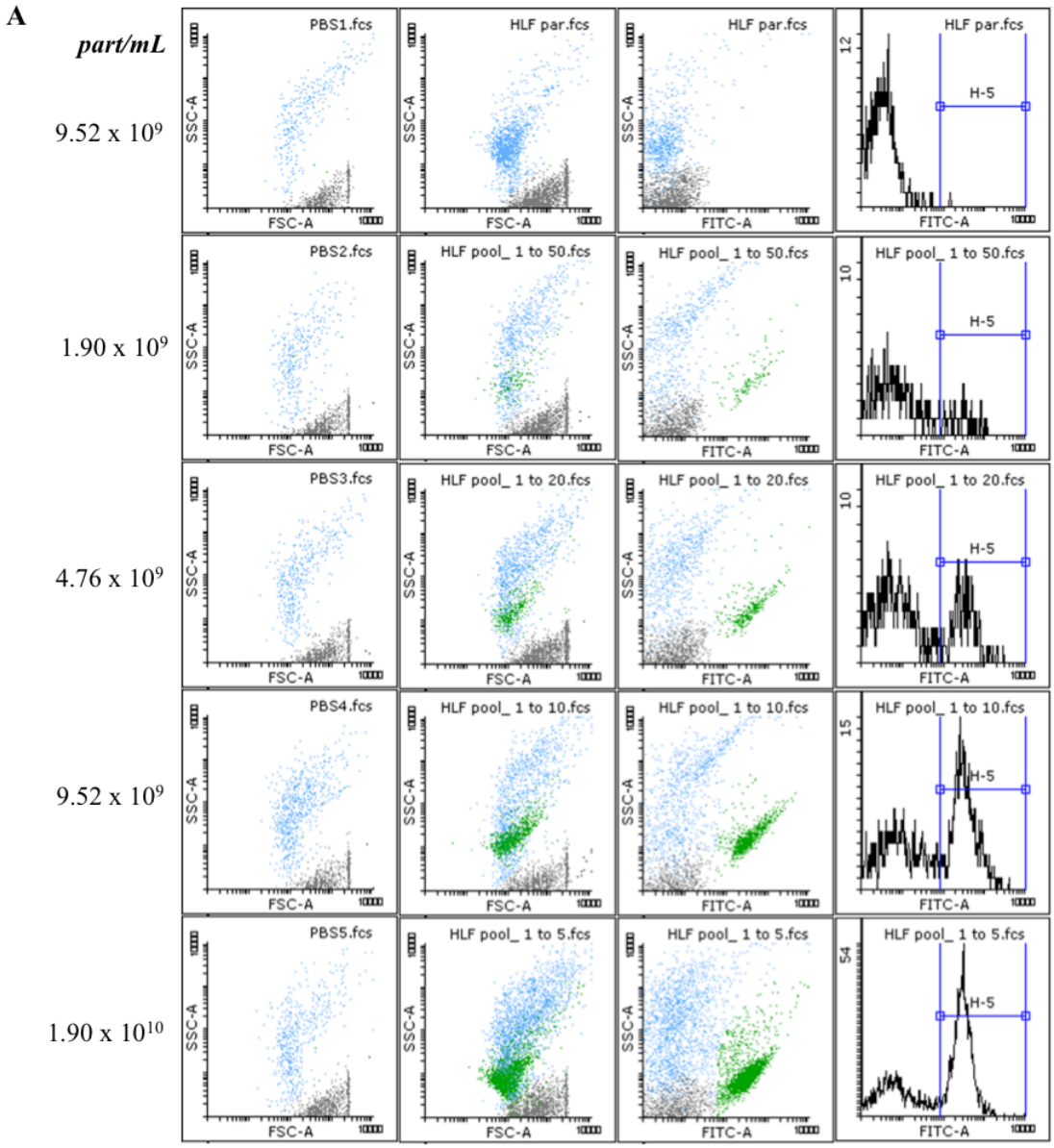

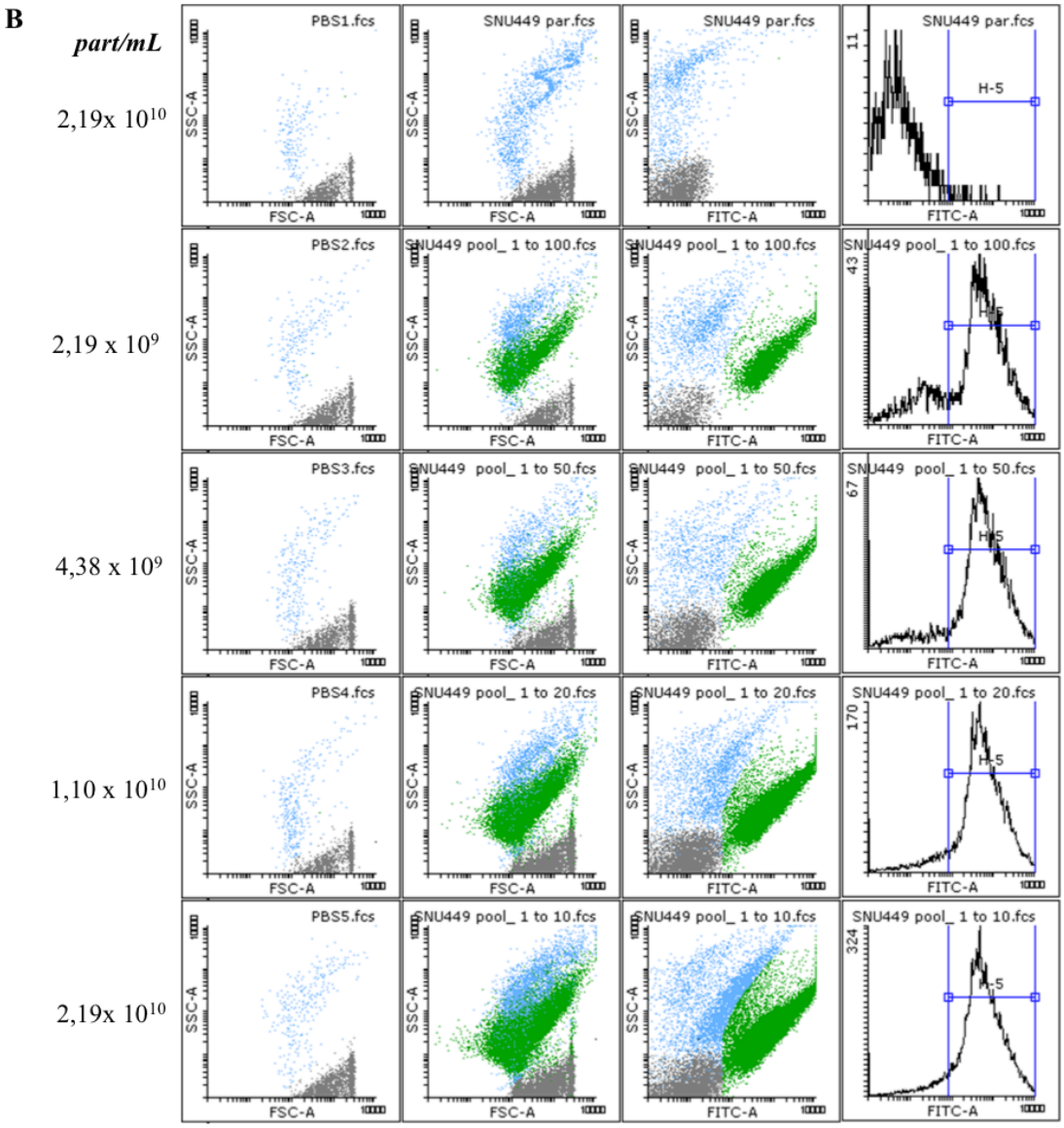

Figure S2. Scatter plots and histograms of increasing particle concentrations of GFP-labeled EVs derived from GFP-CD63-transduced A) HLF and B) SNU449 cells as detected by flow cytometry. Gray, blue and green events represent noise, EV population and GFP-positive EV population, respectively.

LIST OF ABBREVIATIONS

BM-MSCs	Bone Marrow-Mesenchymal Stem Cells
BMPs	Bone Morphogenetic Proteins
CAFs	Cancer-Associated Fibroblasts
CCM	Cell Culture Conditioned Medium
CTCs	Circulating Tumor Cells
DUC	Differential Ultracentrifugation
ECM	Extracellular Matrix
EGF/EGFR	Epidermal Growth Factor/Receptor
EMT-TFs	EMT-Transcription Factors
EMT	Epithelial to Mesenchymal Transition
ERK	Extracellular signal-Regulated Kinase
ESCRT	Endosomal Sorting Complex Required for Transport
EVs	Extracellular Vesicles
HCC	Hepatocellular Carcinoma
HGF	Hepatic Growth Factor
HSCs	Hepatic Stellate Cells
IGF	Insulin like-Growth Factor
IL-1/6	Interleukin-1/6
ITG	Integrin
LSECs	Liver Sinusoidal Endothelial Cells
MAPK	Mitogen-Activated Protein Kinase
MDSCs	Myeloid-Derived Suppressor Cells
MET	Mesenchymal to Epithelial Transition
MFBs	Myofibroblasts
MHC	Major Histocompatibility Complex
MMPs	Matrix Metalloproteinases
mTOR	mammalian Target Of Rapamycin
MVBs	Multivesicular Bodies
NK cells	Natural Killer cells
NTA	Nanoparticle Tracking Analysis
PDAC	Pancreatic Ductal Adenocarcinoma
PDGF	Platelet-Derived Growth Factor
PI3K	Phosphatidilinositol 3-Kinase
SCCs	Single Cell Clones
sEVs	small Extracellular Vesicles
SMAD	Small Mother Against Decapentaplegics
TAMs	Tumor-Associated Macrophages
TDEs	Tumor-Derived Exosomes
TGF-β/ TGFBR	Transforming Growth Factor-β/Receptor
TIMP	Inhibitor of Metalloproteinase
TNF-α	Tumor Necrosis Factor-α
TSG101	Tumor Susceptibility Gene-101
VEGF	Vascular Endothelial Growth Factor
α-SMA	α-Smooth Muscle Actin

LIST OF TABLES

LIST OF FIGURES